3D Shape Memory Alloy Spacer Fabrics

A THESIS
SUBMITTED TO THE FACULTY OF THE GRADUATE SCHOOL
OF THE UNIVERSITY OF MINNESOTA
BY

Chaitanya Damame

IN PARTIAL FULFILLMENT OF THE REQUIREMENTS
FOR THE DEGREE OF
MASTER OF SCIENCE

Dr. Julianna Abel

February, 2024

Acknowledgements

I would like to thank my advisor, Dr. Julianna Abel, for her support throughout the past two years of graduate work. I'd like to thank her for her support, guidance, and direction along with all the impromptu brainstorm sessions, and run-on meetings. I am also grateful for my committee members, Dr. Susan Mantell and Dr. Angela Panoskaltsis-Mortari for their feedback and support.

I would also like to extend my gratitude to all my lab mates, Micheala, Berik, Janghoon, Mohammad Reza, Lakshay and Huxley for all their constructive feedback throughout this project. I would like to especially thank Micheala for helping me muscle through my research and providing insights along the way.

Most importantly, I want to thank my entire family, especially my parents, Nitin and Tejashri, and my sister, Gayatri, for encouraging me to pursue my goals even as they took me far from home. I would also like to thank my family in the US, Himanshu, Siddhant, Saahil, Neha, Shivani, Arushi, Ketki and Pardhu for making my MS journey enjoyable. A special mention to Srujan, who has been an immense support. He has believed in me and has been there for me in difficult times.

This work was supported by an NSF CAREER Award Grant 1943715.

Dedication

To my mother, Tejashri, who has made this possible.

Abstract

The emergence of smart materials is revolutionizing the way we interact with everyday objects by providing additional functionalities to previously conventional devices. As for smart technologies, shape memory alloys (SMA) show significant deformations, large actuation deformations and high energy absorption through thermally dependent solid-state phase transformations. SMA based spacer fabrics have immense potential as energy absorbing structures in areas such as prosthetic socket liners, military backpacks, treatment of pressure ulcers and vehicle seats, but remain limited by obstacles in design and manufacturing. This thesis provides a fundamental understanding of 3D SMA spacer fabrics by investigating the design parameters for their fabrication. The goal of this research is to investigate the impact of textile design (material, geometry and manufacturing) and material effect (superelasticity and shape memory effect) on the mechanical performance of 3D SMA spacer fabrics. Detailed experiments were conducted to analyze the superelasticity and shape memory effect by studying the interactions between different design parameters. We were able to understand the energy absorption through compression in our spacer fabrics. Hence, these fabrics have potential applications in fields of consumer electronics, medicine and sports where energy absorption is key. This research establishes fundamental understanding of SMA monofilaments within spacer architectures and enables us to design, manufacture and characterize 3D SMA spacer fabrics.

Contents

List of Tables

List of Figures

Chapter 1

Introduction

In an era marked by increased urbanization, extreme weather events, and an evolving understanding of health and safety, the demand for innovative solutions to mitigate the impact of external forces on individuals has reached unprecedented levels. Energy-absorbing 3D structures present a unique response to this imperative, offering a versatile and adaptive approach to safeguarding human health in diverse contexts. From sports and recreational activities, where the risk of injuries is inherent, to everyday environments where unforeseen accidents can occur, the capability of these structures to dissipate and absorb energy efficiently positions them as integral components in creating resilient and protective spaces. This research explores the need for innovation in multifunctional 3D energy-absorbing structures and explores their potential in the textile design space.

1.1 Current Energy Absorbers for human health

1.1.1 Prosthetic Sockets

Lower limb prosthesis is often used to restore the appearance and the lost functions of individuals with limb amputation. The prosthetic socket design is crucial for proper fitting, as it facilitates the connection between the residual limb and the prosthesis. The socket design is essential for load transfer, and an improper load application may lead to discomfort or skin damage. Modifying the socket based on residual limb shape,

tissue properties, and load tolerance is crucial for effective load transfer. Along with these sockets, elastomeric liners are used for cushioning and as an interfacial sleeve between the socket and the limb. This interfacial surface is crucial for load distribution. Improper pressure distribution over the socket and the limb can lead to skin ulcers, pain, and irritation in the limb and even affect the gait performance.

Brown et al.[1] discuss an additively manufactured single-layer metamaterial inlay that has variable geometric parameters. The metamaterial inlay reduces peak pressure in the residual limb, which is better in function than silicone liners that are widely used. This additive manufacturing method also highlights the potential for customizable prosthetic liners tailored to the needs of each individual. There have been attempts to design and manufacture personalized liners using cryogenic CNC machining that would conform to the shape of the socket [2]. Current technologies emphasize the customized fit of the prosthetic socket system to mitigate pressure spots, but these systems require constant fit adjustments and have trouble accounting for bodily volume fluctuations[3].

1.1.2 Motor Vehicle Seats

For truck seats, polyurethane foam is used for cushioning as it is low cost and lightweight. The seats must be durable and functionally efficient. The foam seats, however, have limitations. They cannot conform to different shapes of the hips and buttocks. Also, over time, foam cushion degrades, which reduces the cushioning. Foams provide temporary comfort through the cushioning, but over long durations, the foams start to flatten and lose their ability to absorb the pressure, which stresses the drivers' spinal discs [4]. To address this limitation of foam seats, 3D fabrics have been prominently used in car seats over the past few years. Warp-knitted spacer fabrics have proven to have better elastic recovery and air permeability than polyurethane rendering 3D fabrics useful in seat ergonomics [5].

1.1.3 Military Backpacks

Carrying heavy loads is imperative for military personnel [6, 7]. It is possible that the load used can exceed 45% of the body mass [8, 9]. These loads are often known to impact the biomechanics of human gait and affect the efficiency and safety of movement

while posing a high risk of musculoskeletal injury [10, 11, 12]. In military personnel, stress fractures, low back pain, and foot blisters are common problems due to heavy loading.

For heavy load carriage tasks and applications, foot insoles made from polyurethane have mitigated plantar pressure [13]. Insoles made from foam have proven to give comfort during gait however, foams tend to bottom out. Load carriage assistive devices (LCAD) have recently been used in military backpacks [14]. There are different strategies to improve load distribution in load-carrying operations. There are devices that transfer the load to the ground and support the legs and the joints [15], which are external supports that can also be a hindrance during operation. The assistive devices for load distribution are bulky systems and expensive.

1.1.4 Bed Sores/ Pressure Ulcers

Lately, modern wound dressings have been designed to enhance wound healing. Research has shown us the health costs for pressure sores and ulcers are remarkably high [16]. Maintaining blood circulation, avoiding long-continued pressure, and maintaining proper hygiene can prevent bed sores or tissue necrosis. It is difficult for pressure ulcers to heal, and wound dressings that provide good absorption and an optimum cushioning effect are rare. It is estimated that a 10kPa pressure is sufficient to cause tissue death. Owing to this, special cushions are used to distribute pressure over a wide area. These cushions also have semi-fluidic properties that adapt to the shape of the patient's body [17]. The limitation of these foams or cushions is that they eventually flatten.

Recently, weft-knitted spacer fabrics have proven to be a promising textile-based approach as they have tunable physical properties. Owing to their structure and geometry, they have excellent cushioning and are well ventilated, making them helpful in wound healing and pressure ulcer prevention.

1.2 Spacer Fabrics - Textile Approach to Energy Absorption

The applications previously mentioned have one common theme - they absorb energy through the thickness of the structure. One energy-absorbing architecture that has been

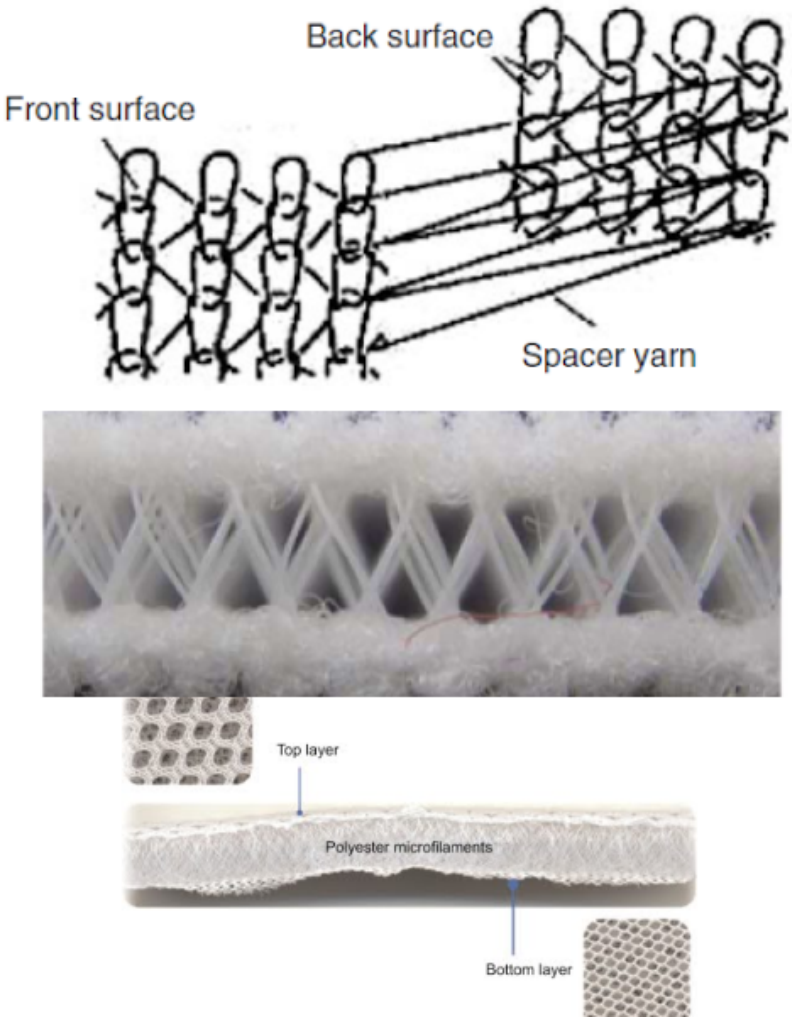

Figure 1.1: General spacer fabric consisting of two faces that are connected by a spacer yarn [18, 19]

around for a long time is spacer fabrics. A spacer fabric consists of two surfaces that are held apart by a spacer yarn. Figure 1.1 shows 3D spacer fabrics having a front face and a back face that is connected by a spacer yarn. 3D spacer fabrics represent a transformative advancement in textile engineering, offering a departure from conventional two-dimensional fabrics. These innovative textiles are characterized by a unique structure composed of multiple layers interconnected by spacer yarns. This distinctive

construction not only imparts three-dimensionality to the fabric but also introduces a range of benefits. Open spaces within the fabric enhance breathability, making it well-suited for applications requiring ventilation and comfort. The layered structure also provides superior cushioning properties, making 3D spacer fabrics ideal for protective gear, automotive interiors, and medical applications. The versatility of these fabrics, coupled with their ability to combine comfort with functionality, positions them at the forefront of textile innovation, with applications spanning various industries.

1.2.1 Spacer Fabrics - State of the Art

Multi-layer Warp-knitted Spacer Fabrics (Multi-layer WKSFs)

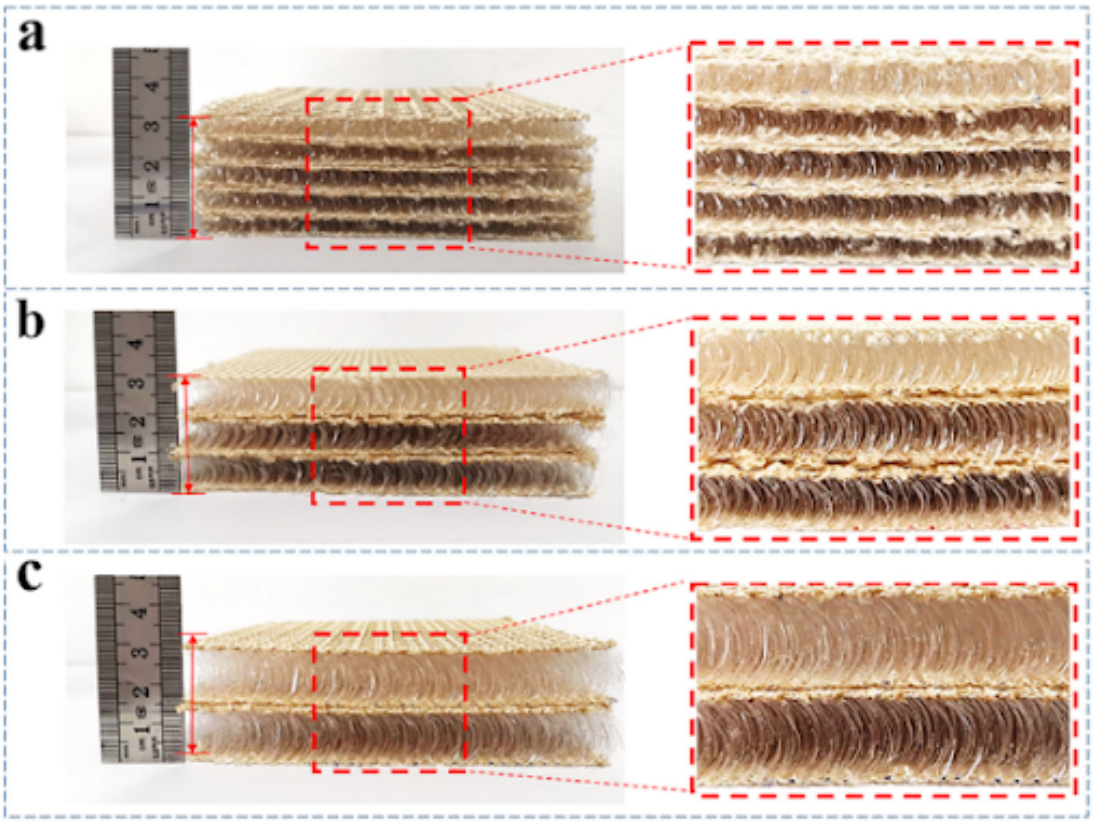

Figure 1.2: Multi-layer warp knitted spacer fabrics (WKSF)[20]

Spacer fabrics are known to have immense tunability through their geometry. Yu

et al.[20] talk about the compressive and low-velocity impact properties of three kinds of WKSFs with multi-layers. Figure 1.2 shows the three different types of WKSFs manufactured by Yu et al. From the compression tests, it was found that the energy absorption was the highest in WKSF with more layers (Sample A). From the fatigue-compression resistance tests it was found that Sample A had better fatigue resistance and had a low strain. However, from the low-velocity impact test, Sample C, with just two layers, absorbed more energy. Hence, they concluded that for low-velocity impacts on the human body, two-layered WKSFs can be used for protective applications.

Silicone tube inlays in spacer fabrics

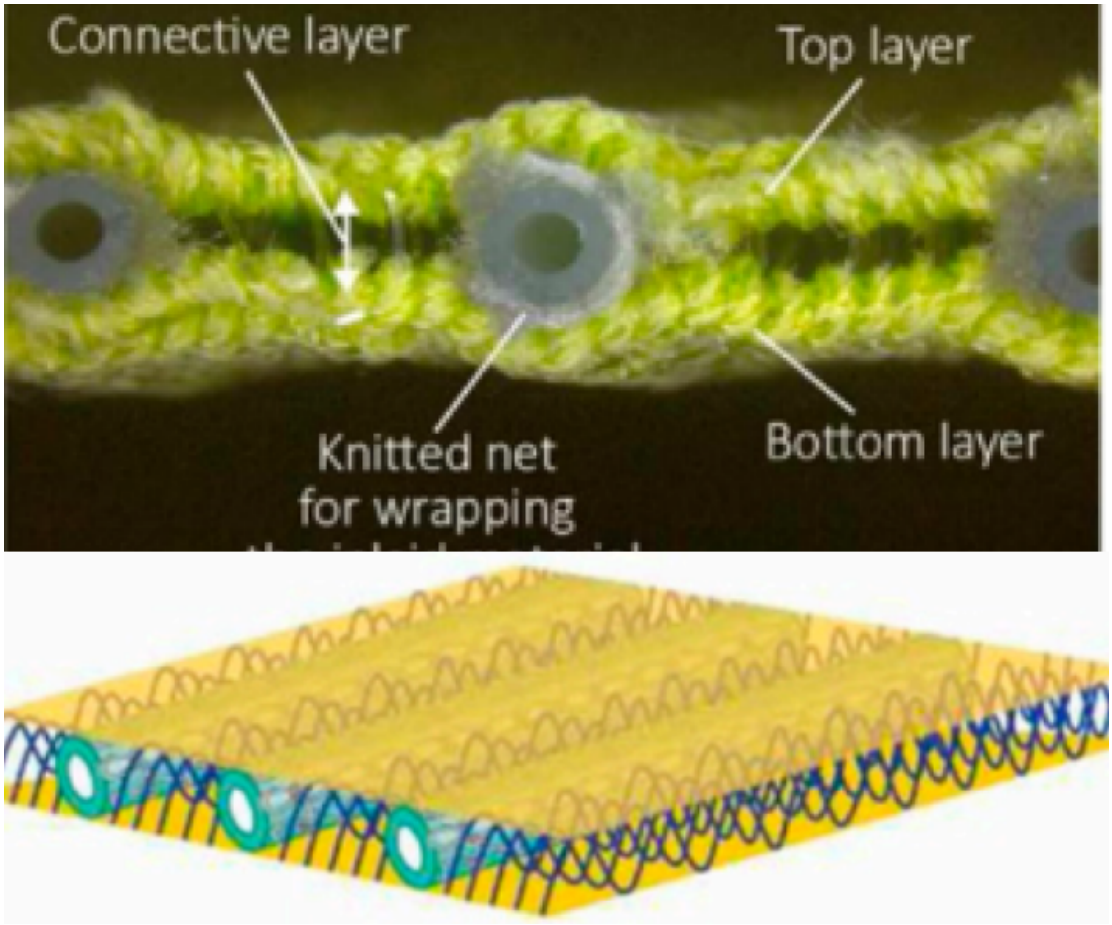

Figure 1.3: Silicone tube inlays for improving cushioning in spacer fabrics[21]

Li et al. [21] discuss a novel approach of integrating silicon tube and foam inlays to improve cushioning in weft-knitted spacer fabrics (shown in Fig. 1.3). It was found that the inlays can effectively enhance the impact force reduction of the 3D spacer fabrics. The air permeability, thermal conductivity and impact force reduction of the inlaid spacer structure can be modified with changes to the diameter of the spacer yarn, type of inlay and net material used and spacer pattern, whilst its water vapor permeability can also be varied by using different types of inlays. Insoles made with the proposed inlaid spacer structure not only reduce the magnitude of the plantar pressure but also preserve a breathable in-shoe environment to facilitate heat dissipation, reduce plantar temperature, humidity from sweating and even ulcers. The findings from this study provide useful guidelines that can broaden the applications of inlaid spacer fabric for cushioning apparel and footwear in clinical and sports applications.

Manufacturing methods for making functional spacer fabrics

Figure 1.4: Warp knitting and Braiding technologies for spacer fabric manufacture[22]

Textile triboelectric nanogenerators (TENGs) can be integrated in traditional textiles with the help of the advanced three-dimensional (3D) warp-knitted structure. A

scalable and washable 3D warp-knitted spacer power fabric (3D-WSF) with high compression elasticity and enhanced power output was developed. The 3D-WSF can also act as a self-powered sensor that can monitor human motions, such as walking states and sitting postures. This manufacturing method, shown in Figure 1.4, has enabled the making highly functional 3D spacer fabrics which have potential applications in wearable power supply and self-powered sensors. This work provides a new 3D smart textile structure for TENGs, which may promote the application of textile TENGs in wearable micro/nano power sources, self-powered sensors, and human–machine interfaces [22].

3D Weft-knitted spacer fabrics with NiTi monofilaments

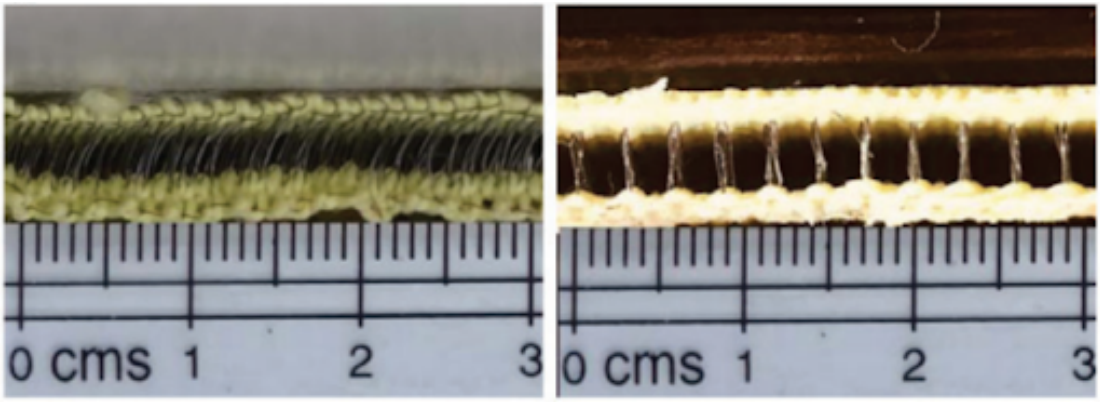

Figure 1.5: Weft-knitted spacer fabrics with NiTi monofilaments[23]

Hamedi et al. [23] investigated the optimum design of a weft knitted 3D spacer fabric (shown in Fig. 1.5) as cushioning material for protective applications, specifically for ultimate use in offloading insoles for persons with diabetes. They carried out compression tests and the quasi-static tests results showed that for high stress levels, spacer fabric with shape memory alloy (NiTi) wires as spacer yarn, exhibited significantly better cushioning behavior compared to samples with polyamide and steel spacer monofilaments. They also studied effects of spacer architecture and type of shape memory alloy materials on energy absorption and cushioning behavior. They concluded that 3D weft knitted fabrics with coarse shape memory alloy (SMA) monofilament spacers in higher-inclined patterns are the most suitable option for cushioning pad in protective equipment. The knitted spacer fabric with SMA spacer yarn can be utilized in medical

applications such as orthopedic insoles for diabetic patients or impact-imposed sports activities. This research shows the material tunability and its effects on 3D spacer fabric performance.

1.2.2 Shape Memory Alloy (SMA) Spacer Fabrics

Integration of SMA monofilaments as a spacer fiber unlocks myriad tunable physical and material properties of the textile system. The SMA-monofilament spacer fabric will have the compression properties similar to that of conventional spacer fabrics, but also have an actuation potential and better stress recovery as a result of shape memory effect. With a 3D SMA integrated spacer fabric, one can combine the high stiffness, large recoverability and hysteretic damping of SMA knitted in a lightweight textile architecture, resulting in high mechanical energy absorption.

Hamedi et al. [23] discuss the cushioning properties of a 3D weft-knitted spacer fabric in a novel design with NiTi monofilaments. It was seen that SMA spacer fabrics had better cushioning behavior compared to spacer samples made from polyamide and steel as spacer yarns. The paper also discusses the effects of spacer fiber diameter and spacer fiber geometry on the energy absorption for cushioning applications. The paper proposes the use of 3D SMA spacer fabrics as orthopedic insoles for diabetic patients and impact-imposed sports activities. This research paves the way into the space of 3D SMA spacer fabrics as energy-absorbing structures.

This work discusses a fundamental approach in energy absorption in 3D SMA spacer fabrics. However, the paper only discusses the superelastic behavior of these 3D SMA spacer fabrics. Also, the research does not include the study of the actuation potential of these spacer fabrics. They study the effect of slope and inclination angles of the spacer fibers in the spacer architecture for cushioning and energy absorption. From this work, we understand that 3D SMA spacer fabrics have tunability in their design through material, structural, geometric and manufacturing parameters. We can explore the impact of 3D SMA spacer fabrics as energy absorbing structures through textile design and the material effect of shape memory alloys in 3D spacer architectures.

1.3 Goal Statement and Objectives

The goal of this research is to investigate the impact of textile design (material, geometry, manufacturing) and material effect (superelasticity and shape memory effect) on the mechanical performance of 3D SMA spacer fabrics. The following research objectives are crucial in order to achieve this goal.

1. Fabricate 3D SMA spacer fabrics.
2. Test the 3D SMA spacer fabrics for energy absorption.
3. Explore the actuation potential of 3D SMA spacer fabrics.
4. Isolate the impact of different geometric parameters on the performance of 3D SMA spacer fabrics.

Chapter 2

Materials and Structures

2.1 Shape Memory Alloys

Shape memory alloys (SMA), such as nickel-titanium (NiTi), are a class of materials that exhibit a solid-state phase transformation between martensite and austenite, known to produce large actuation forces, contractions, and recoverable strains [24]. This solid-state phase transformation occurs when the material is heated to a B2 cubic austenite (A) phase from either a monoclinic temperature induced self-accommodating twinned martensite phase (TIM, M^t) or from a detwinned stress-induced martensite phase (SIM, M^d)(shown in Fig. 2.1.a). Owing to these reversible, solid-solid, diffusionless thermoelastic phase transformations, SMA demonstrates interesting phenomena like the shape memory effect (SME) and superelasticity (SE) [25]. The transition between the austenitic and martensitic lattices can be introduced through thermal (SME) and mechanical (SE) loading. The phase transformations are characterized by transformation temperatures; martensite start (M_s), martensite finish (M_f), austenite start (A_s), and austenite finish (A_f). The phase transition properties can be customized through changes in chemical composition and heat treatments such as annealing [26].

Actuation contraction is caused by the shape memory effect (SME) which is shown in Figure 2.1.b. SME is defined as the capability of SMA to return to a predetermined shape on heating. It is driven by the recovery of material strains from the change of lattice structure between the deformed martensite and the memorized stiffer austenite. The memorized austenitic shape can be customized through thermal processing to

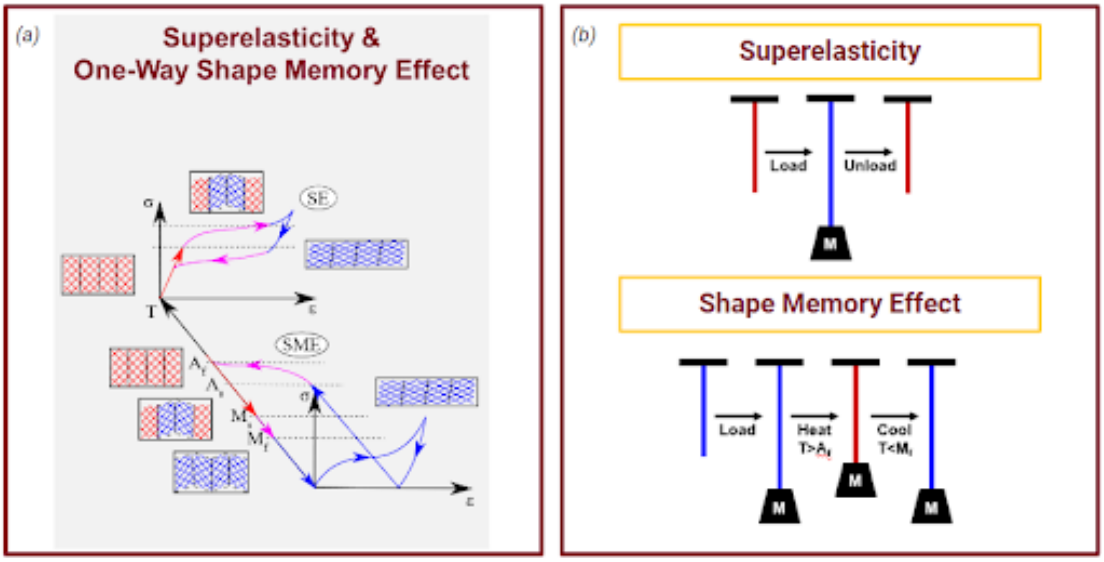

Figure 2.1: Shape Memory Alloys Phases and Behavior (a) The superelastic (SE) and shape memory effect (SME) are based on the reversible solid-to-solid phase transition between the high-symmetry austenite and low-symmetry martensite phases as functions of the applied temperature, strain, and stresses [25] (b) Superelasticity (SE) is the ability to recover large strains (about 8%) and associated large stress-strain hysteresis due to mechanical loading-unloading under isothermal conditions. Shape Memory Effect (SME) is defined as the capability of SMA to return to a predetermined shape on heating.

shape-set material geometry and relieve material stresses from geometric deformations. Superelasticity (SE) is the ability to recover large strains (about 8%) and associated large stress-strain hysteresis due to mechanical loading-unloading under isothermal conditions. The superelastic effect is observed during loading in the hot austenitic phase (T¿A_f), where the solid-state transformation to a stress-induced detwinned martensitic phase is mechanically introduced. The forward A→M^d transformation is bounded by a near-constant stress plateau. Upon unloading, the reverse M^d→A transformation occurs, signified by a constant stress plateau but at a lower stress than the forward transformation. The superelastic effect allows SMAs to recover up to 8% structural strain, which is a unique trait of SMA-based systems. Also, the inner loop, showing hysteretic transformations between the loading and unloading curves amounts to the energy dissipated as heat. It also goes to show the multifunctionality of SMA-based

systems for damping or harvesting energy. The strong dependence of multifunctional SMA performance on material stress and strains enables easy performance enhancements through geometric reconfiguration [27].

2.2 Spacer Fabric Construction

Spacer fabric is a three-dimensional knitted fabric consisting of two separate knitted faces that are joined together or kept apart by spacer (or filer) yarns [28]. Spacer fabrics are a category of knit structures that have a unique cushiony feel, are breathable, and have a low density [29]. There are two kinds of knitted spacer fabrics, warp-knitted and weft-knitted. They are classified based on the method of knitting and the specific knitting machines. Warp knitted spacer fabric is a three-dimensional textile made on a double-needle bar Raschel machine [30] Weft knitted spacer fabrics can be made using two ways, either on a double jersey circular machine having a rotary needle cylinder and a needle dial [28] or on a flat-bed knitting machine.

2.2.1 Planar Weft Knitting

Two-dimensional (2D) weft knitting is a common textile manufacturing technique that involves the interlocking of horizontal rows of yarn to create a flat, planar fabric. A series of knit loops and purl loops, shown in Figure 2.2.a, form a pattern of loops which give us a 2D knitted structure.This process is typically carried out on a flat knitting machine, which consists of a bed of needles arranged horizontally. The machine shown in Figure 2.2.b is a flat bed weft knitting machine. As the carriage moves back and forth on the knitting bed, the needles move up and down interlocking with the yarn to form loops, creating the fabric. The direction of the knitting is perpendicular to the direction of yarn feeding, resulting in a 90-degree angle between the fabric rows and columns. In 2D weft knitting, the vertical columns of loops are called "wales," and the horizontal rows are referred to as "courses." (shown in Fig. 2.2.c)The combination of wales and courses determines the fabric's structure and characteristics. For this research, we implemented this technique to make the face rows of the spacer fabric. The knit pattern used is called "stockinette", which is shown in figure 2.2.c.

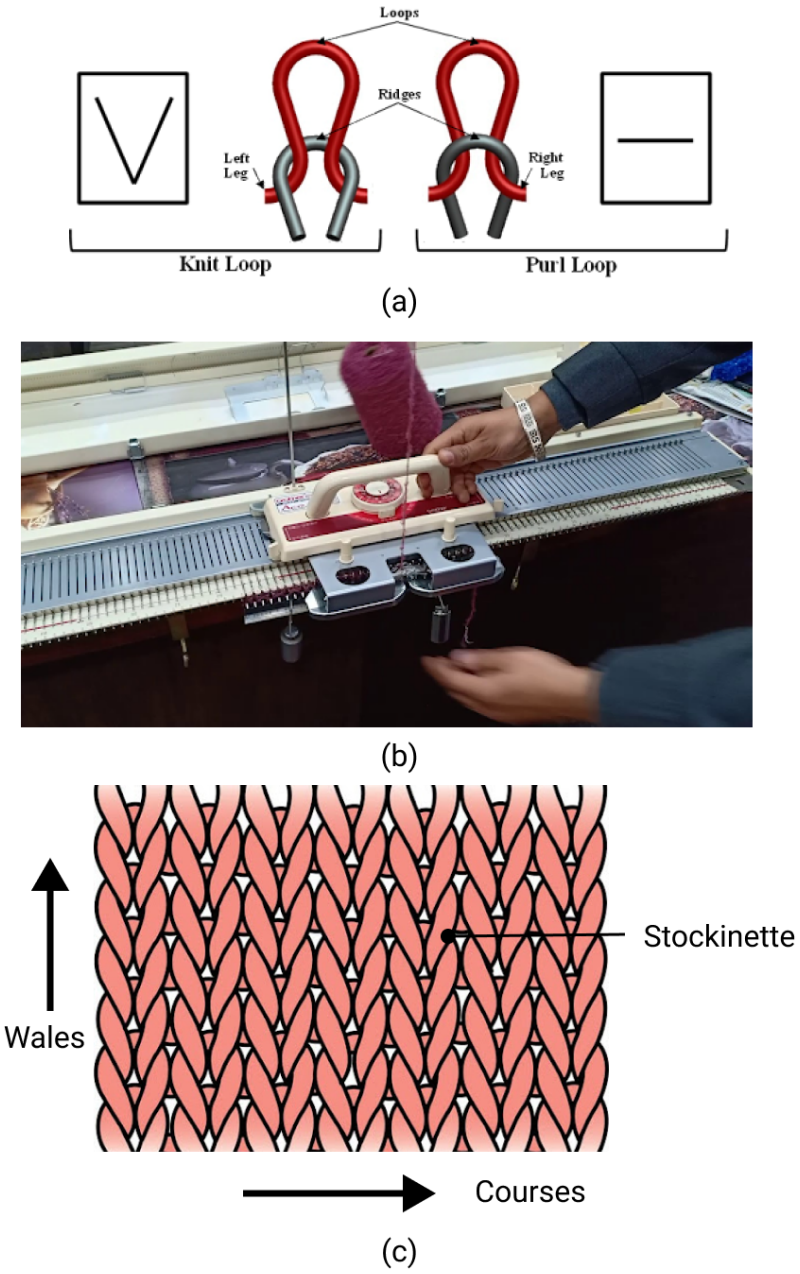

Figure 2.2: a) Knit and Purl loops b) Flat-bed weft knitting machine for making 2D planar weft- knitted fabrics. c) Stockinette pattern used to make face of the spacer fabric

2.2.2 Circular Knitting

Traditionally, knitting 2D structures is done on a flat-bed weft knitting machine. For my project, I modified the traditional weft knitting approach to make a 3D spacer fabric. In order to achieve this, the flat bed knitting machine needs to be set up with the ribber attachment shown in Figure 2.3. With the ribber attached, the machine is now in the

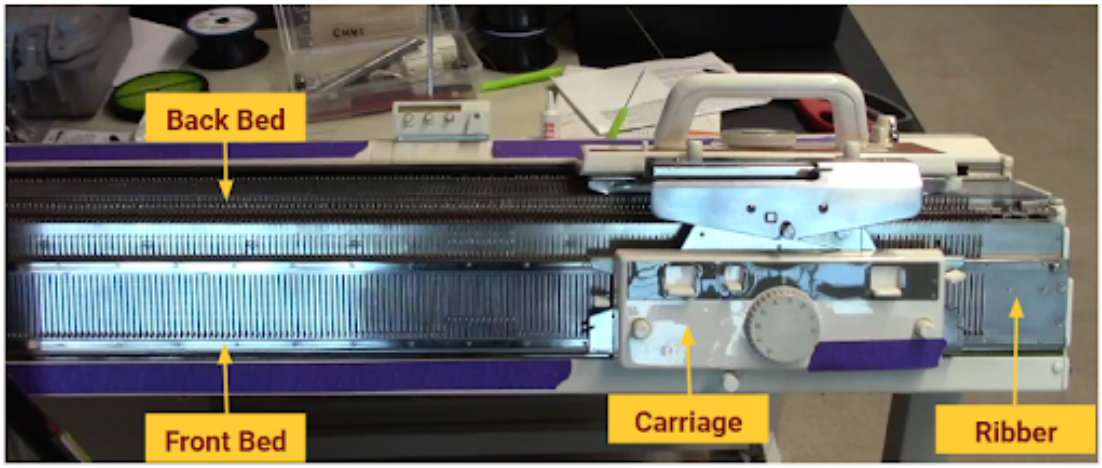

Figure 2.3: Taitexma TH860/TR850, Design of Active Materials and Structures Lab

V-bed configuration. In this arrangement, one can knit using both the knitting beds, the front bed and the back bed. The carriage is used for knitting on the beds. The yarn from the yarn feeder goes into the carriage. The knitting operation starts from the right. The yarn engages with the needles on the front bed as the carriage moves from right to left. Now, as we move the carriage from left to right, the needles on the back bed are engaged by the carriage, which knit loops on the back bed. As the yarn is fed continuously, this back and forth movement of the carriage forms face loops of the yarn on each bed. This continuous knitting operation enables us to knit on both the beds simultaneously in a circular fashion. This is called circular knitting. I used this knitting technique for making the front face and the back face of the spacer fabric.

2.2.3 Tuck Operation

Using circular knitting, we can knit the front and back faces of the spacer fabric. In order to knit between the two faces, the technique that I used is called tucking. In

tucking, the spacer yarn is alternated between the front and back beds. In tucking, no new face rows are formed. Figure 2.4 shows the tuck operation. After knitting one face

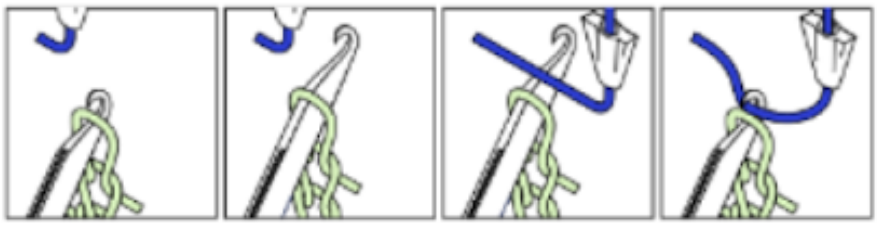

Figure 2.4: Tuck Operation [29]

row with circular knitting, the spacer yarn is tucked into the needle hooks alternating between both the beds. This enables us to keep both the faces apart from each other.. After knitting one face row and one tuck row, we can continue the same sequence to form a 3D spacer fabric using a V-bed weft knitting machine.

In the industry, spacer fabrics are usually produced on warp knitting machines that are characterized by dedicated yarn feeders for each needle in a bed which makes the machines quite large and has a bulky setup overhead. They are suitable for making large and consistent fabrics. However, this method of knitting has very little within-fabric programmability. On the other hand, weft knitting allows us tunability in the production parameters of the fabric on a stitch-by-stitch basis [29].

2.2.4 Manufacture of Spacer Fabrics on a V-Bed Weft Knitting Machine

A v-bed weft knitting machine produces knit fabric on two straight rows (beds) of hook-shaped needles [29]. Spacer fabric knitting proceeds by alternating between two basic steps.

In the first step, face rows are formed using sequences of the knit operation. Rows are added to both the front and back faces, which are knit on the front and back beds respectively. While knitting, going from right to left, needles engage on the front bed, hence knitting only half of the row. On moving from left to right, the needles on the back bed are engaged, completing the circular knit. Moving from right to left and back

to the right completes one circular row. At this time, the two faces of the fabric are separated by only the small gap between the two needle beds.

In the second step, filler rows are added at the same needles using the tuck operation, which incorporates the yarn into the stitch without forming another row of fabric. By tucking at a regular interval onto alternating beds, the filler yarn forms a shallow lengthwise zig-zag. Because tucking does not add height to the fabric, subsequent passes of filler yarn add density to the same face row of the fabric. Figure 2.5 shows the construction of a 3D spacer fabric.

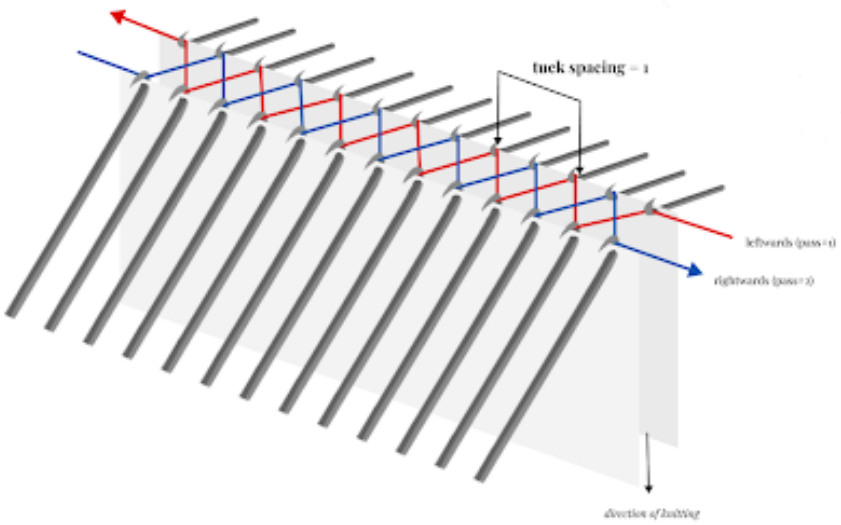

Figure 2.5: 3D Spacer Fabric Construction

Figure 2.6 shows the 3D SMA spacer fabric that was manufactured in the lab using the Taitexma TH860/TR850. The faces are knit with a passive yarn, Kevlar, which is in tension at knitting time. After knitting, the tensioned passive yarn in the faces causes them to shrink laterally. This shrinkage pulls the filler yarn zig-zag in, pushing the faces apart into the characteristic "fluffy" thickness of the spacer fabric, giving it the cushiony effect.

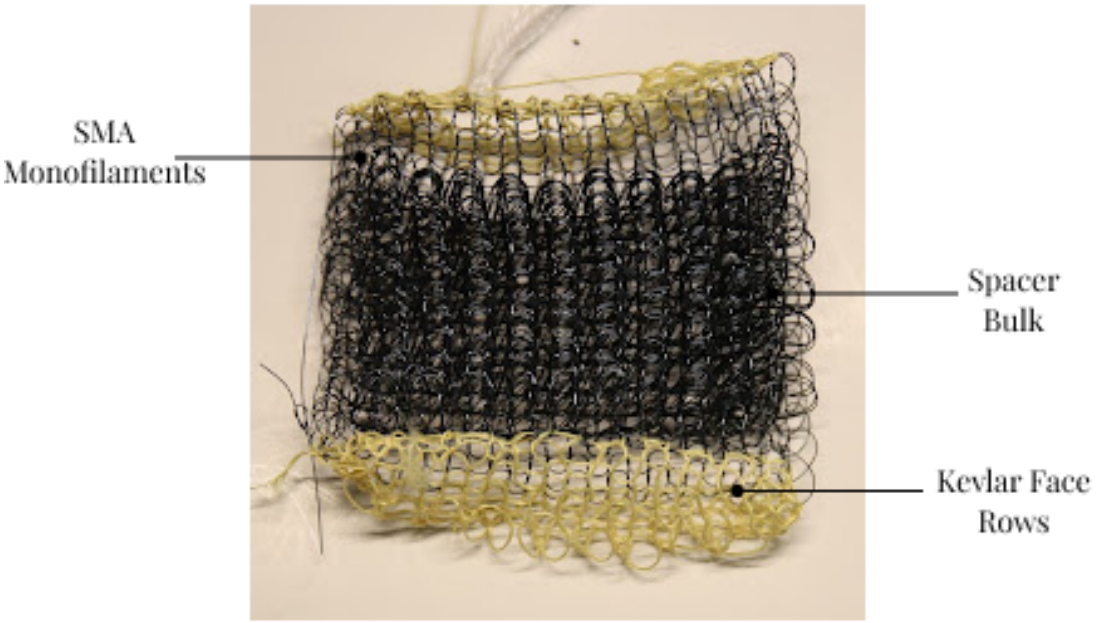

Figure 2.6: 3D Spacer Fabric Construction

Chapter 3

Design of Experiments and Experimental Methodology

3.1 Fabrication Parameters

Spacer fabrics have mechanical properties that are interlinked with different aspects of the spacer fabric architecture. The fabrication of spacer fabrics is dictated by three main parameters namely material parameters, geometric parameters and machine parameters. Material parameters are the different types of yarns and fibers having different diameters, elastic moduli etc. that are used for the faces and spacer bulk. Geometric parameters are face loop sizes, row density, tuck spacing etc. which define the spacer fabric architecture. Lastly, the machine parameters are factors such as needle spacing, needle alignment, distance between the knitting beds, yarn tension etc. that are exclusive to the fabrication setup (knitting machine).

3.1.1 Material Parameters

The material parameters include the different yarns and fibers that were used in the spacer fabric manufacture. The spacer fabric has two main component yarns, the face yarns and the spacer monofilaments. The face yarn is used to create the front and back faces of the spacer structure. We used Kevlar as a cast-on and cast-off material. The diameter of the Kevlar yarn was 0.015", which was the smallest diameter available at the

time. As these spacer samples are thermally actuated, Kevlar is used as the sacrificial (cast-on/cast-off) yarn as it has a high heat resistance. Even though Kevlar is slightly stiffer than other knitting yarns such as wool and cotton, it is possible to perform machine knitting with it. Apart from the sacrificial face yarns, the spacer monofilament was used for knitting the faces of the spacer bulk. We used DYNALLOY Flexinol wire, shown in Figure 3.1, with a transition temperature of 70^{o}C for the spacer monofilaments as well as the spacer monofilament faces. We used two different wire diameters, 0.006" and 0.008". The subsequent sections explain the manufacture of these spacer fabrics.

Figure 3.1: Dynalloy Flexinol wire spools for 0.006" and 0.008" wire diameters and transition temperature = 70^{o}C

3.1.2 Geometric Parameters

These are the parameters that are tunable. The geometric parameters considered for the fabrication were tuck spacing, spacer row density and tuck pattern offset.

Tuck spacing is the distance in needles between a filler yarn tuck and the next tuck on the same bed. The Figure 3.2 shows tuck spacing for four different values. For our research we only manufacture samples with tuck spacing of 0 and 1. On our machine, the tuck spacing greater than 2 was difficult to manufacture. As the distance between

the needles increases, clean tuck formation cannot be achieved on our knitting machine.

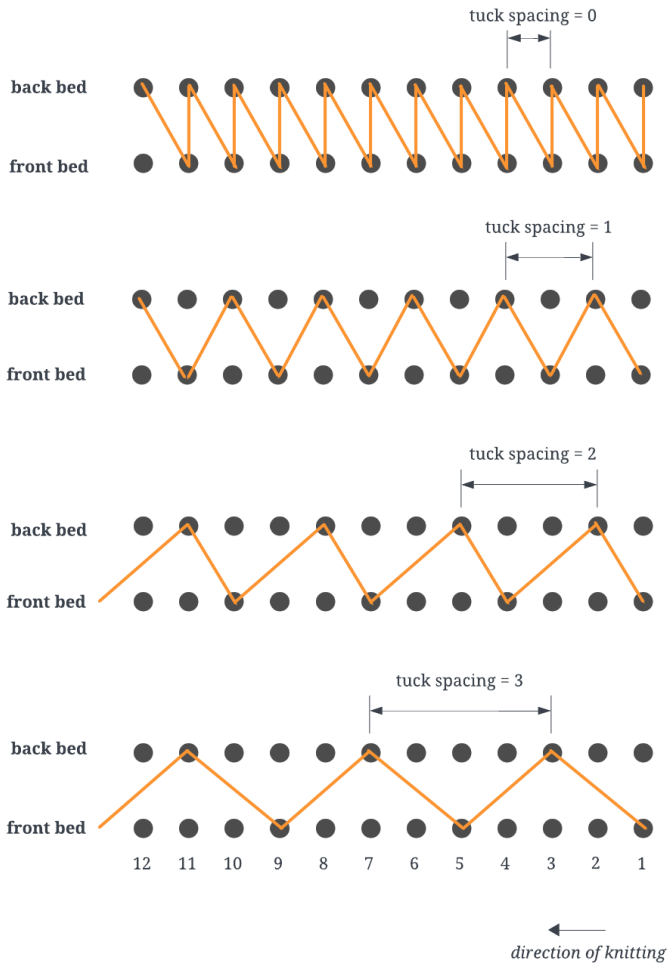

Figure 3.2: Tuck Spacing. Shows the top view of the knitting beds for different values of tuck spacing. In our research, we only use tuck spacing = 0 and tuck spacing = 1 for the design of experiments

Spacer row density is defined as the ratio of spacer rows to rows of face fabric height. In knitting, every row has a direction of formation (leftward or rightward)

which must be alternated.(shown in Figure 3.3) To greatly simplify the programming of these structures, we always pair a leftward pass with a rightward pass; therefore, for the scope of this research, in all our examples, the number of rows of each spacer fabric sample made is always even; we factor out this duplication in expressing the filler row density as a ratio. Hence, our samples will have a ratio of either 1/1 or 2/1 (filler rows passes/face rows passes). For this DOE setup, we chose to make samples with 2 passes and 4 passes as they were easy to manufacture on our knitting machine. Also, increasing the number of passes makes the sample heavy and the tuck operation becomes difficult.

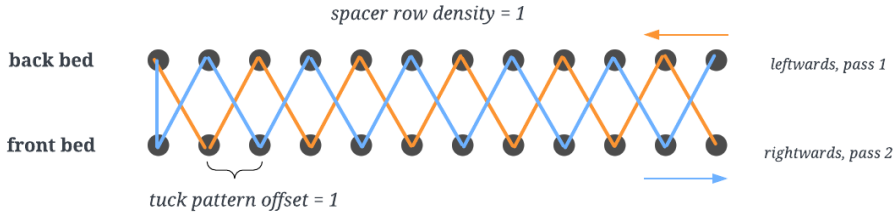

Figure 3.3: Spacer Row Density and Tuck Pattern Offset. Shows two passes of the spacer monofilament in one row. No. of spacer rows passes = 2 and no. of face rows passes = 2, hence spacer row density = 2/2 =1. Also, the tuck positions in pass 1 is offset by one needle in pass 2. This gives us a tuck pattern offset = 1

Tuck pattern offset is given as the distance in needles between the tuck positions in one pass and the tuck positions in the previous pass. For the scope of this research, we have limited the tuck pattern offset to one. (the tuck is offset by one needle).

3.1.3 Manufacturing Parameters

For the manufacture of the spacer fabrics, Taitexma TH 860/TR 850 manually-driven knitting machine with the ribber attachment, i.e. in the V-bed configuration, was used. The manufacturing parameters were driven by the knitting machine configuration. Factors such as needle spacing, distance between the knitting beds, needle alignment, yarn tension and loop size were considered for the fabrication.

Needle spacing is the distance between two adjacent needles on the same knitting

bed. The Taitexma TH860/TR850 has a needle spacing of 4.5mm. For our machine shown in Figure 3.4 , the needle spacing is fixed.

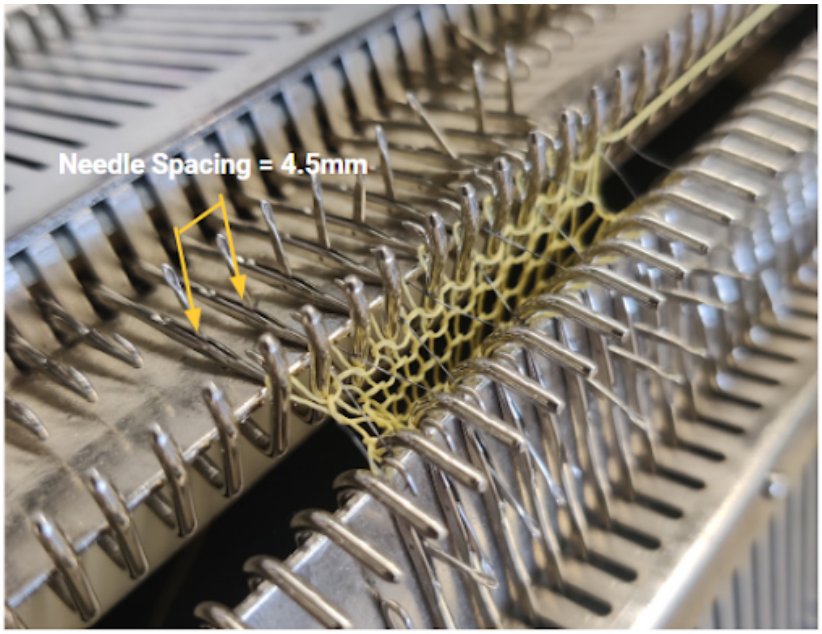

Figure 3.4: Needle spacing on the Taitexma TH860/TR850

The distance between beds is another factor that affects the thickness, stiffness, and energy absorption of a spacer fabric. The distance between the front and back beds was 10mm on our machine and it was fixed, shown in Figure 3.5. This ensured that all the spacer samples had a similar initial thickness.

Needle alignment is the alignment of needles on one bed with respect to the needles on the other bed. Depending on the machine, the ribber can be set in two positions; in-line, where the needles on opposite beds are in line with one another, or offset, where the needles are offset from one another. The Figure 3.6 shows the “in-line” and “offset” configurations on the Taitexma TH860/TR850. For the simplicity of design, all the spacer fabric samples for this research were manufactured with the ‘in-line” setting.

As for the yarn tension, it is sometimes possible to control the tension on the yarns during knitting. For the scope of this research, the knitting beds were used as fixtures for knitting. The knitting operation for the face yarns and the tucking operation for the spacer monofilaments were both done manually. The knitting machine has a constant

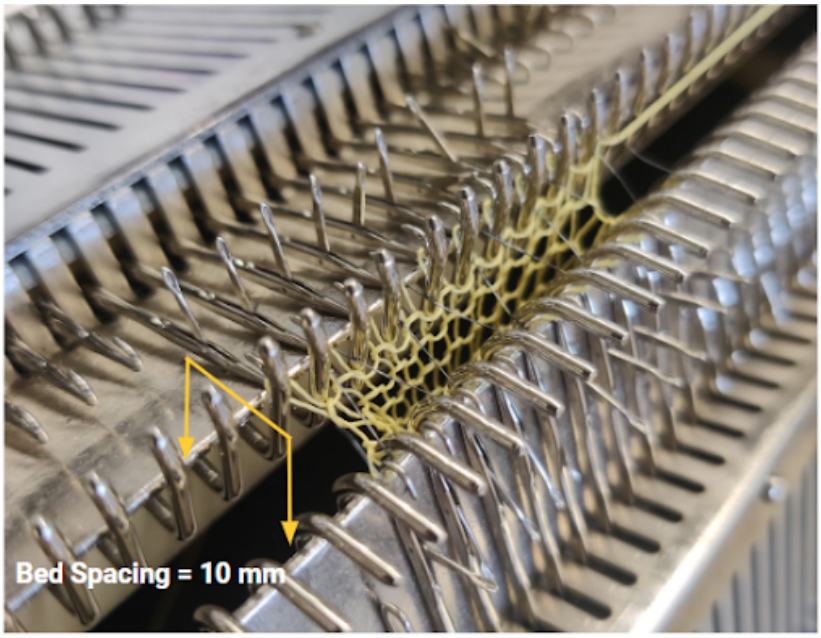

Figure 3.5: Bed spacing on the Taitexma TH860/TR850

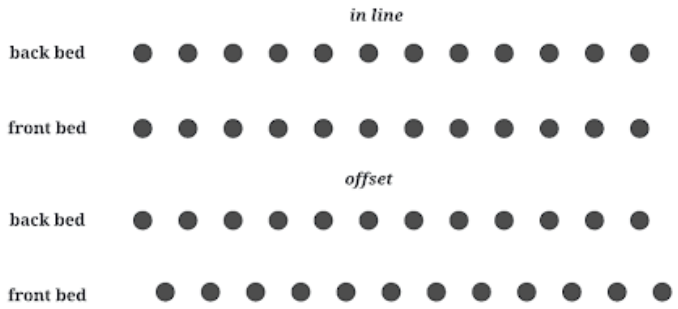

Figure 3.6: Needle alignment on the Taitexma shown in two configurations,"in-line" and "offset"

needle alignment and a constant distance between the two knitting beds. Lastly, the face loop size is the size of knitted face loops produced by the knitting machine. It arises from a combination of factors, including yarn tension, needle spacing, the distance between needle traverses and the material of the yarn used. For this research, the loop size was not considered as a primary geometric parameter that could alter the spacer fabric

performance.

3.1.4 Design of Experiments - Full Factorial (2^n)

A two-level full factorial Design of Experiments (DOE) having 3 main factors was developed. The Table 3.1 shows us the high(+) and low(-) values of the main factors for our design.

Main Factor	**Low (-)**	**High (+)**
Fiber Diameter	0.006”	0.008”
Tuck Spacing	0	1
Spacer Row Density	2 passes	4 passes

Table 3.1: Main Factors for DOE

The eight samples were manufactured using the parameters outlined in Table 3.2.

Trial	**Fiber Diameter (in.)**	**Tuck Spacing**	**Spacer Row Density**
Sample 1	0.006”	0	2
Sample 2	0.006”	0	4
Sample 3	0.008”	0	2
Sample 4	0.008”	0	4
Sample 5	0.006”	1	2
Sample 6	0.006”	1	4
Sample 7	0.008”	1	2
Sample 8	0.008”	1	4

Table 3.2: Full Factorial DOE

Table 3.3 gives the DOE setup in the high (+) and low (-) configurations. Eight spacer samples were made based on the full factorial DOE mentioned above. The knit pattern for the faces was a simple circular knitting pattern. All the samples were manufactured at the Design of Active Materials and Structures Laboratory at the University of Minnesota on the Taitexma TH 860/TR 850 manually-driven knitting machine with a fixed needle spacing of 4.5mm. All the samples consisted of 18 horizontal courses and 12 vertical wales for the active spacer geometry, shown in Figure 3.7. The entire sample consisted of 28 horizontal courses (5 courses with sacrificial material at the top and bottom each) and 12 vertical wales. Figure 3.8 shows three spacer fabric samples from

Trial	Fiber Diameter (in.)	Tuck Spacing	Spacer Row Density
Sample 1	-	-	-
Sample 2	-	-	+
Sample 3	+	-	-
Sample 4	+	-	+
Sample 5	-	+	-
Sample 6	-	+	+
Sample 7	+	+	-
Sample 8	+	+	+

Table 3.3: DOE Setup

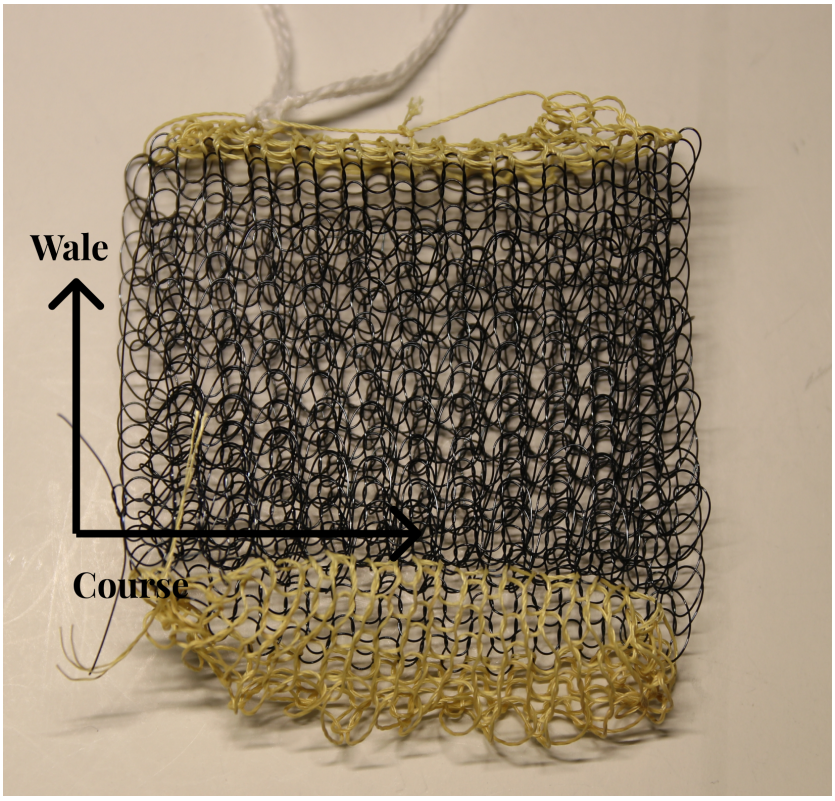

Figure 3.7: 3D SMA Spacer Fabric - Courses and Wales

the eight sample DOE. We can see that the samples 2, 4 and 5 are made with different parameters.Due to different fiber diameters and tuck spacings, the samples have slightly different lengths. Sample 4 has a spacer row density = 4, which makes it look denser

compared to samples 2 and 4.

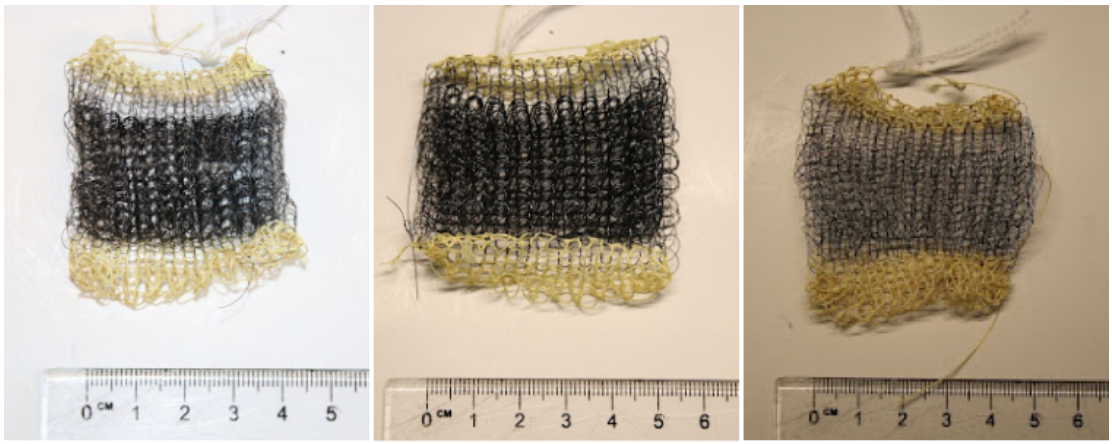

Figure 3.8: 3D SMA Spacer Fabric - Sample 2 (fiber diameter = 0.006", tuck spacing = 0, spacer row density = 2), Sample 4 (fiber diameter = 0.008", tuck spacing = 0, spacer row density = 4) and Sample 5 (fiber diameter = 0.006", tuck spacing = 1, spacer row density = 2)

3.2 Experimental Setup

The prepared spacer samples were tested for energy absorption and for actuation displacements. The tests were performed in the Polymer Characterization Facility at the University of Minnesota, Twin Cities. The tests were conducted in the RSA G2 Rheometer by TA Instruments shown in Figure 3.9.

Compression tests were performed in the RSA G2 for the eight spacer samples. Two 25mm circular platens were used as the compression fixture. The top platen was connected to a motor and a pressure transducer. The bottom platen was fixed and did not move upon operation. The sample was placed between both the platens, ensuring there was no contact between the fabric surface and the platens when zeroing the load transducer. The compression fixture is shown in Figure 3.10.

Figure 3.9: RSA G2 Rheometer at the Polymer Characterization Facility, University of Minnesota

3.3 Experimental Procedure

3.3.1 Isothermal Compression Test

SMA spacer samples have material properties that are thermally dependent, which results in different energy-absorbing capacities at different temperatures. To investigate

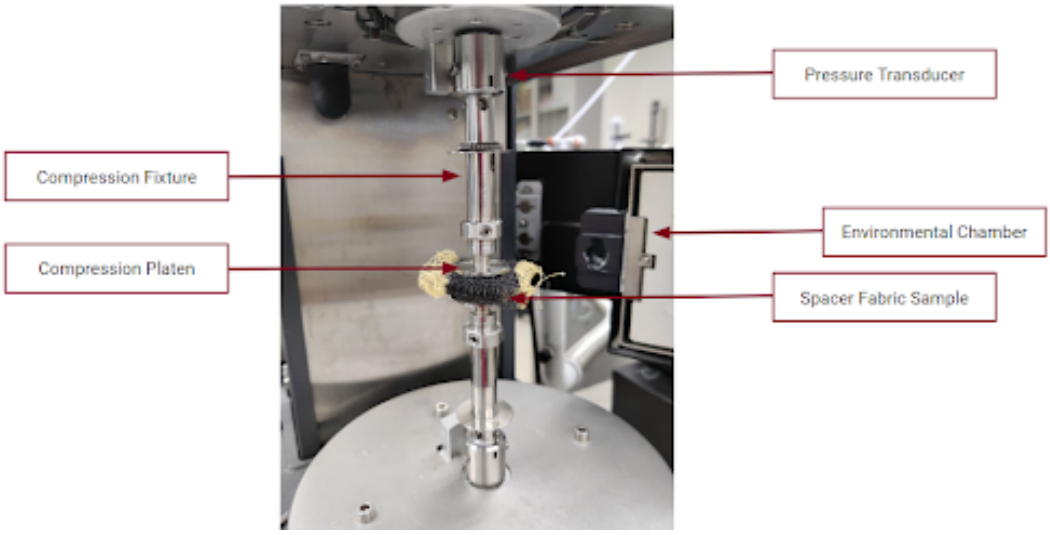

Figure 3.10: Compression Fixture Setup

the energy absorption in the spacer fabrics, an environmental chamber was used to regulate the temperature during the experiment. Isothermal compression tests were performed on all the samples at two different temperatures. The austenitic mechanical performance was evaluated at 120^{o}C and the martensitic mechanical performance at 20^{o}C. These temperatures were identified on the past tests conducted in our lab for SMA wires [27, 31]. At 120^{o}C, the sample was compressed at a constant strain rate for about two-thirds of the original thickness. After complete loading (compression), the unloading (de-compression) was also conducted at the same pace, keeping the temperature constant. The same cycle was repeated, first loading and then unloading, at 20^{o}C. All the samples were tested for austenitic mechanical performance at 120^{o}C and for martensitic mechanical performance at 20^{o}C. The following steps explain the isothermal compression test performed on one sample:

- After zeroing the transducer and the gap between the platens, introduce the sample between the platens.
- Ensure that the platens just touch the sample and then close the environmental chamber.
- For austenite, set the temperature to 120^{o}C. For martensite, set the temperature

to 20^{o}C.

- Adjust the gap between the platens to ensure that the pressure transducer reading is zero.
- Note the gap height (thickness).
- For loading, set the limit to $2/3^r d$ of the gap height. We only compress the sample to 66.67% of its initial height.
- Calculate the linear compression rate for this height. The strain rate= 4x10$^-$4 s$^-$1 is constant.
- Start the test. Loading and unloading take place at the same rate.

Figure 3.11 shows one loading-unloading cycle as recorded in the DMA. As the loading begins, the force acting on the sample (blue) increases. The distance between the compression platens starts decreasing (green), changing the gap height of the sample. After reaching the $2/3^r d$ compression height, the unloading begins. We can see that the force starts decreasing as the compression platens go away from each other and the gap height goes on increasing. From this data, we get one compression-decompression cycle.

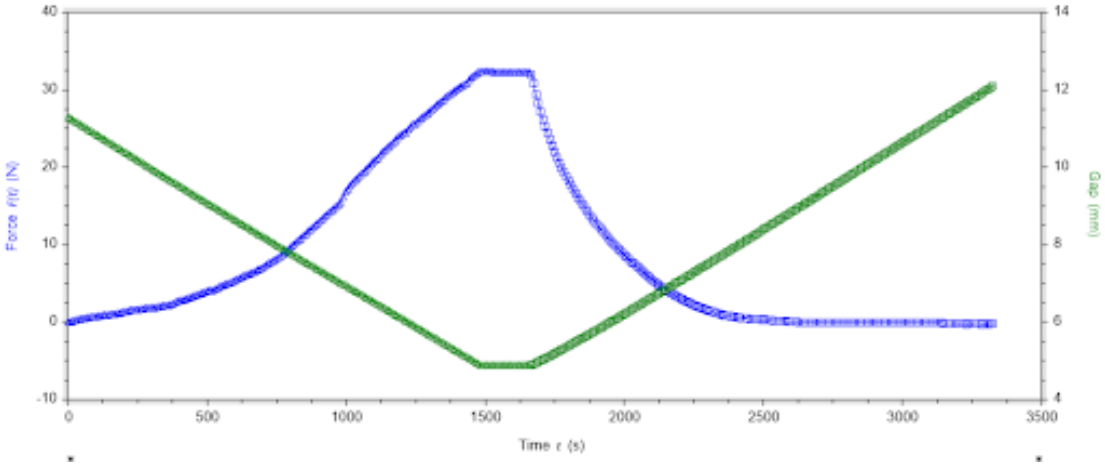

Figure 3.11: Loading and unloading cycle recorded in the DMA during the isothermal compression test

The pressure transducer measures the axial force during the loading-unloading cycle along with the changing height between the compression platens. Figure 3.12 shows a force vs. gap height plot that we get from the DMA. We record two such plots for one sample, one for the hot state (120^{o}C) and other for the cold state (20^{o}C). We use this data to calculate the compressive stress and compressive strain in the spacer fabric.

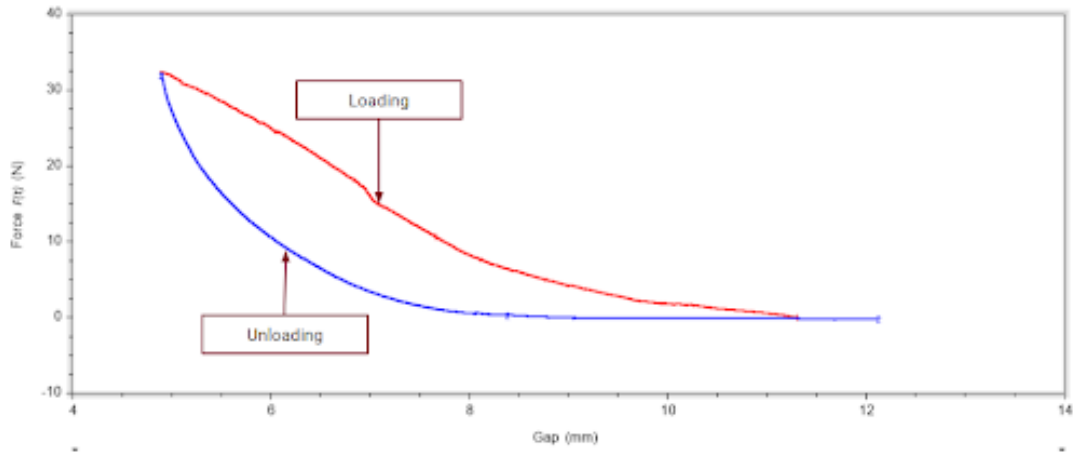

Figure 3.12: Force vs. gap plot measuring the loading and unloading force with the changing gap height

As SMA has different elastic moduli at different temperatures, different architectures made from the same SMA material can have different stiffnesses. The mechanical behavior is also unique at different temperatures. Also, the amount of energy absorbed may also vary depending on the strain rate at which the samples were compressed. For this test setup, the environmental chamber was set at 120^{o}C. The tests were only conducted for a spacer fabric sample in austenite. During the fabrication process, our samples have significant deformations that prevent the material from fully transitioning to austenite. Three different strain rates were identified and were categorized as fast, medium, and slow, are given in Table 3.4.

Slow Rate	4 x 10$^-$4s$^-$1
Medium Rate	5.5 x 10$^-$3s$^-$1
Fast Rate	4 x 10$^-$2s$^-$1

Table 3.4: Different strain rates at which Sample 5 replicates were tested

Only one sample, Sample 5 (wire diameter = 0.006", tuck spacing = 1, spacer row density = 2), with quadruplicates was used for this experiment. Each spacer fabric sample was tested at three different strain rates, one after the other. The sequence of the different rates was not the same with all the samples.

3.3.2 Constant Force Temperature Ramp Test

This test was performed to study the actuation potential of these 3D SMA spacer fabrics. The samples were subjected to a constant force while the temperature in the environmental chamber was alternated between 120^oC (sample in austenite) and 20^oC (sample in martensite). This setup helped us understand if the sample could do thermally-induced mechanical work against the constant force, due to the shape memory effect demonstrated by SMA.

For this particular experiment, the environmental chamber was connected to the liquid nitrogen oven setup. We wanted to study the actuation from martensite to austenite, so the temperature of the chamber needed to fluctuate from 120^oC to 20^oC and then back to 120^oC, to complete one cycle of testing. While the temperature changed, either rise or fall, the sample was compressed at a constant pre-defined force. Each sample was tested for five forces, which were calculated based on the maximum austenite load.

The following steps explain the constant force temperature ramp test for one sample:

- After zeroing the transducer and the gap between the platens, introduce the sample between the platens.
- Ensure that the platens just touch the sample and then close the environmental chamber.
- Set the initial temperature to 120^oC.
- Adjust the gap between the platens to ensure that the pressure transducer reading is zero.
- Note the gap height (thickness).

- From the isothermal tests, identify the max. force recorded during the austenite cycle.
- Using that force range, calculate five force values (f1, f2, f3, f4, f5 , where f1¡f5). We use these values as force constants.
- Set the environmental chamber to alternate from 120^{o}C to 20^{o}C and then back to 120^{o}C,for one force value.

For each new test cycle, the force was increased from the previous cycle while having the temperature go from 120^{o}C to 20^{o}C and then back to 120^{o}C. Each sample went through 5 cycles with increasing forces with subsequent cycles.

Figure 3.13 shows the data collected by the DMA after the constant force temperature ramp test for one spacer fabric sample. The plot shows the changing gap height (green) as the temperature alternates between 120^{o}C and 20^{o}C (red) while a constant force (blue) acts on the sample. For a given constant force, the gap height decreases as the temperature decreases (sample becomes cooler) from 120^{o}C (A1) . After the temperature reaches 20^{o}C (M), we let the sample soak in that temperature for 3 minutes. Now, the sample is in the martensite state. As the temperature starts increasing, the sample pushes the top compression platen, doing mechanical work against the constant force. We can see that the gap height recovers almost fully when the temperature reaches back to 120^{o}C (A2). We see temperature-induced actuation in the spacer fabric, which confirms shape memory effect in 3D SMA spacer fabrics.

We use this data from the DMA to plot actuation displacements induced in the samples as temperatures go from A1-M-A2. Figure 3.14 shows the actuation displacements for Sample 1. We can see that for a given constant force, as we vary the temperature from A1 to M, the sample undergoes change in height (displacement). We see that the sample almost recovers this displacement, when the temperature rises from M to A2.

3.4 Calculations

3.4.1 Isothermal Compression Test

From the RSA G2 Rheometer, we get the axial force (N) and the change in gap height (mm). In order to process the data testing data, we need to calculate the compressive

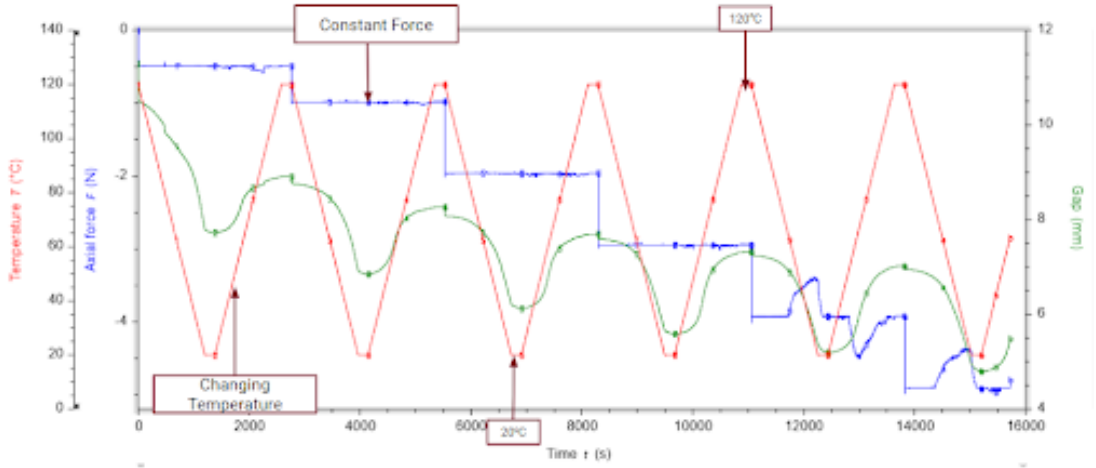

Figure 3.13: Constant force temperature ramp test for sample 1. The plot shows the changing gap height (green) as the temperature alternates between 120^{o}C and 20^{o}C (red) while a constant force (blue) acts on the sample

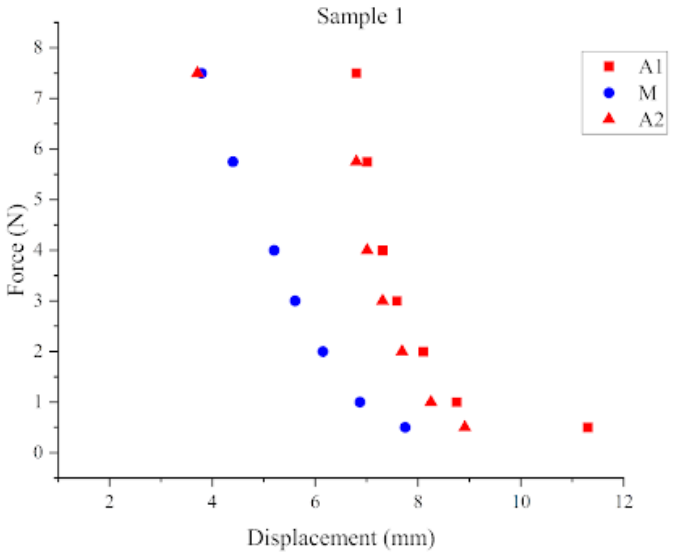

Figure 3.14: Force vs. displacement plot showing the shape memory effect in Sample 1 as the temperature decreases from A1 (120^{o}C) to M (20^{o}C) and the recovers back at A2 (120^{o}C)

stress and the compressive strain for each sample.

The compressive stress is given by,

$$Compressive\ Stress = \frac{Axial\ Force(\boldsymbol{N})}{Area\ under\ the\ platen(\boldsymbol{mm^2})} \tag{3.1}$$

We get the axial force reading from the transducer directly. The area of the platen is calculated from the diameter of the compression platen used, i.e. 25mm. The compressive stress calculated here is only the stress in the active region of the spacer fabric under the platen.

The compressive strain is given by,

$$Compressive\ Strain = \frac{Change\ in\ initial\ gap\ height(\boldsymbol{mm})}{Initial\ gap\ height(\boldsymbol{mm})} \tag{3.2}$$

All the samples have a different initial gap height and hence the strain values are calculated based on these values individually for all the samples.

From the stress and strain values, we plot the stress-strain curve for each sample. The area under this curve gives us the energy absorbed by the spacer fabric. These values were used to plot absorbed energy vs. stress, giving us the energy absorption profile for each spacer fabric.

Chapter 4

Results and Discussion

4.1 Passive vs. SMA Spacer Fabric Performance

Two control samples were produced with passive materials to assess the impact of the active material on the performance of the spacer fabrics. These control samples were made with Kevlar yarn and Polyamide monofilament. The Kevlar yarn had a diameter of 0.015" and the Polyamide was 0.02". These samples had almost double the fiber diameter as that of SMA. As discussed by Hamedi et al.[23], the general compressive behavior of passive spacer fabrics is given in Figure 4.1. The curve indicates that the behavior has three stages. The first stage comprises two segments. Initially, a gradual curve with a lower slope is observed, indicating the unrestricted post-buckling of spacer monofilaments. Subsequently, a steeper slope follows, denoting the linearly elastic phase where the post-buckling of spacer monofilaments is constrained by continued compression and increasing constraints. In the second stage (plateau phase), two phenomena occur, each exerting opposing effects on deformation force, ultimately leading to a nearly constant deformation force across a wide range. The first phenomenon involves an increase in deformation force due to the reduced effective length of monofilaments caused by increased compression. The second phenomenon entails a decrease in deformation force resulting from the torsional and shear deformation of the spacer monofilament. Finally, in the last stage (densification), a rapid escalation in deformation force is observed due to the contact between monofilaments and with outer layers, leading to densification. Figure shows the compressive stress-strain relationship of SMA spacer fabric and pas-

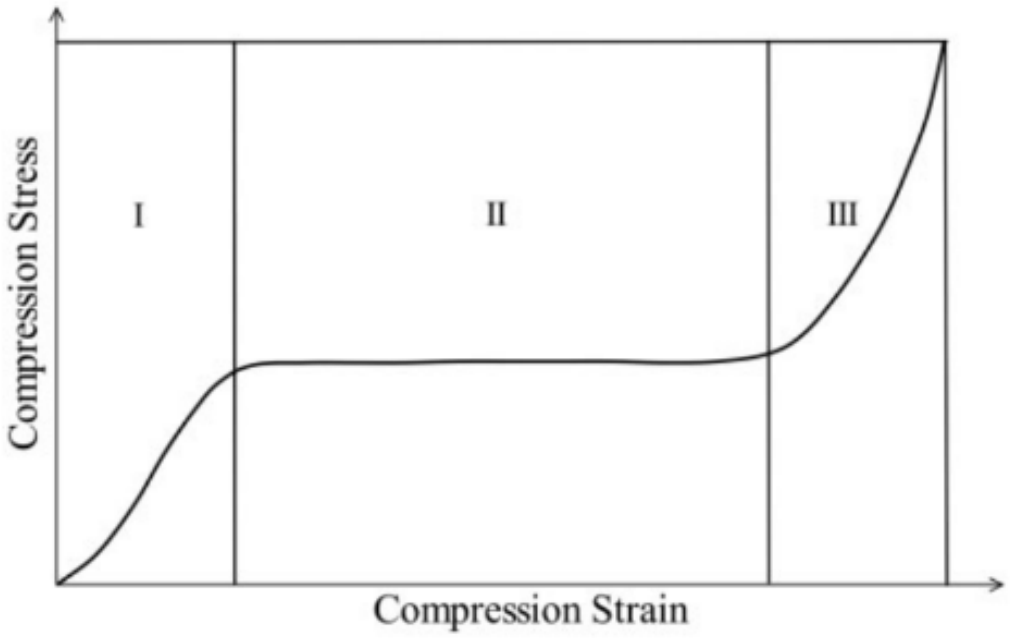

Figure 4.1: General compression behavior of 3D spacer fabric[23]

sive control samples made from steel and polyamide. We tested one sample each made of Kevlar, Polyamide, and SMA, with a tuck spacing of 1, spacer row density of 1, and a tuck pattern offset of 1. All these samples were tested at 20^oC. We wanted to confirm the compression behavior shown by Hamedi et al. and see if our testing protocols gave similar results.

We saw that all the samples had a similar stress-strain curve discussed by Hamedi et al., which can be seen in Figure 4.3. At 20^oC, the SMA spacer fabric is martensitic and is not as stiff as the passive control sample made from Kevlar or Polyamide. The Kevlar sample seems to have a larger hysteresis area compared to the other two samples. A larger hysteresis area means greater energy absorption. Hence, we plot the absorbed energy vs. compressive stress for the same samples. Figure 4.3 shows the absorbed energy for samples made from Kevlar, Polyamide, and SMA.

The energy absorption plot (Fig. 4.4) shows that the polyamide control sample has much better energy absorption than the SMA spacer fabric at stresses above 15

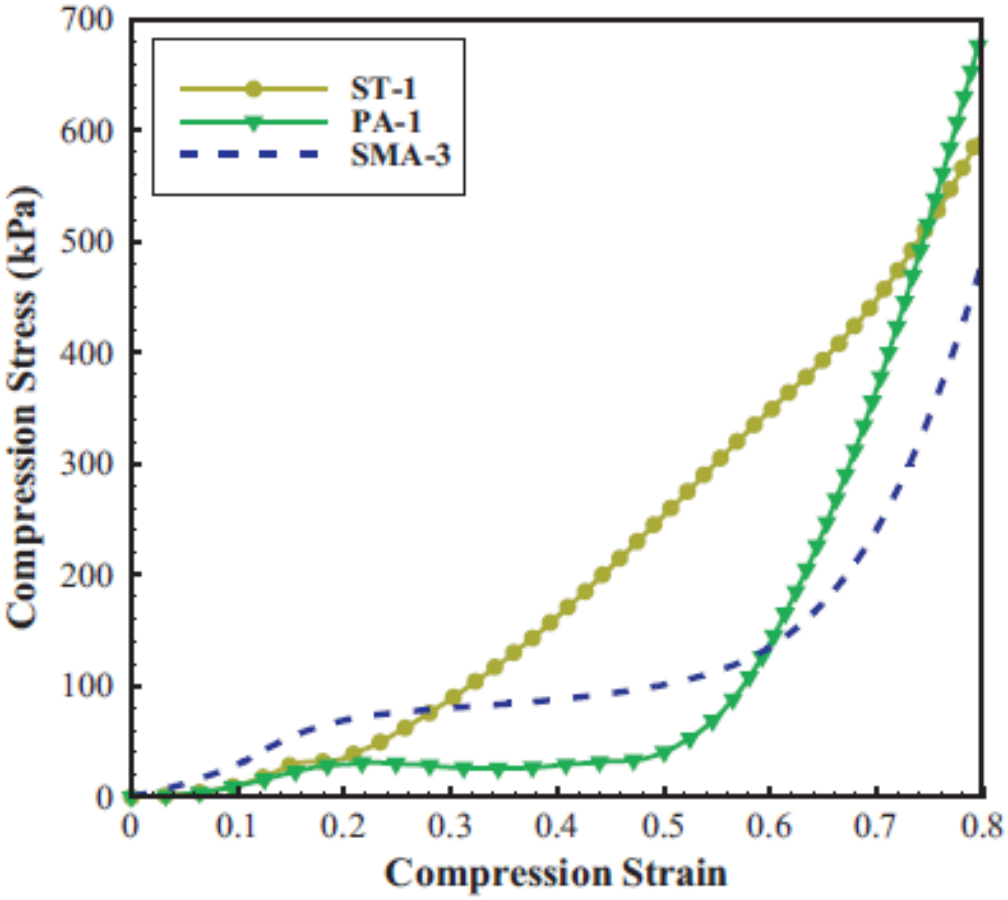

Figure 4.2: Compressive behavior of 3D spacer fabrics made with Steel, Polyamide and SMA [23]

kPa. Additionally, the Kevlar sample absorbs more energy, 4.5 kJ/m^3 compared to 3.0 kJ/m^3 over the range of strains tested. However, as the absorbed energy increases with increasing stiffness, it is worth exploring the energy absorption of the SMA spacer fabric when in the austenite phase. When SMA is heated above its austenite finish temperature becomes stiffer compared to its cold, flexible martensitic phase.

Hence, we further tested the SMA spacer sample at 120^{o}C. The SMA wire used had a phase transition temperature of 90^{o}C. After heating the sample to 120^{o}C, we let

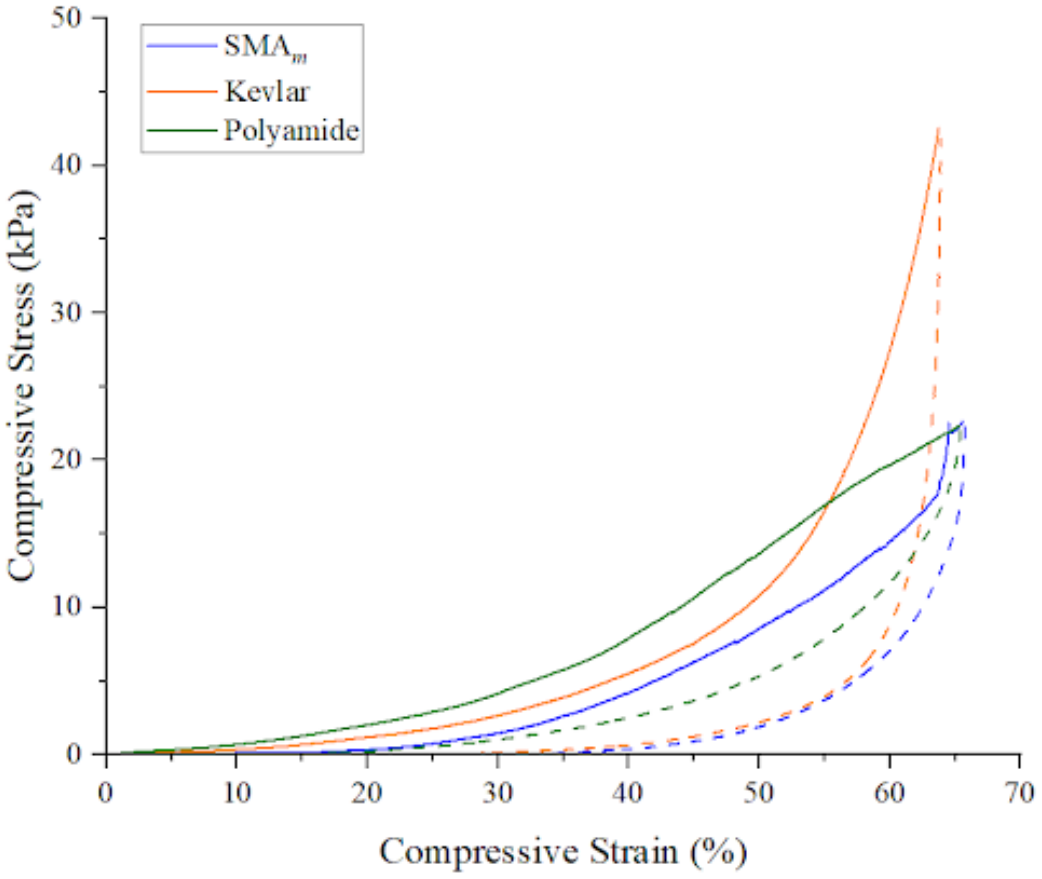

Figure 4.3: Stress-strain curves for SMA spacer sample and passive control samples made from Kevlar and Polyamide

it soak at that temperature for about 10 minutes. We plotted the compressive stress-strain curve for the higher temperature austenite phase alongside the previous curves (Figure 4.5). At higher temperatures, the SMA spacer sample becomes stiffer than in the cold, martensite phase. Also, it has a wider hysteretic curve compared to the other samples, which increases the energy absorption by the sample. The SMA sample in the hot state absorbs 16 kJ/m^3 at a maximum strain of 66% of the initial thickness. This is more than three times the energy absorbed during 66% compression of the samples at 20^{o}C. This is interesting as we have two different performance curves for the same SMA sample.

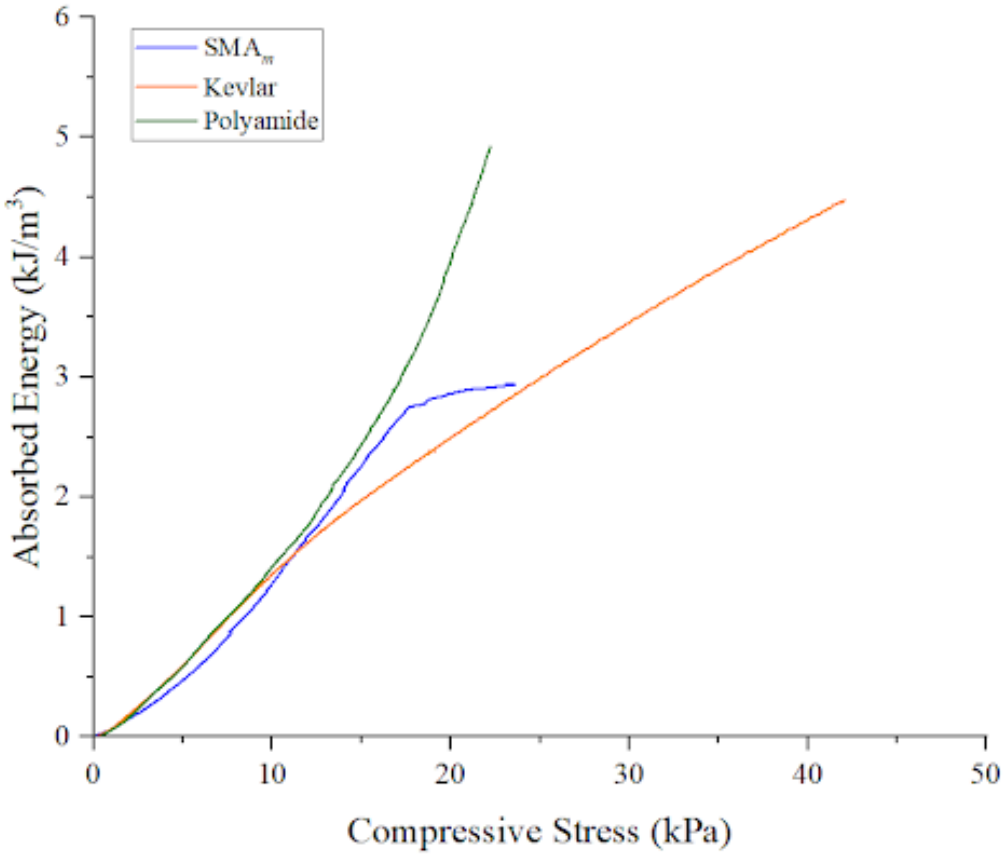

Figure 4.4: Absorbed energy in SMA, Kevlar, and Polyamide samples

After all the tests, it was observed that the Kevlar and Polyamide samples had permanent deformation. The passive control samples "flattened-out" after their initial use. On the other hand, the SMA sample in the cold state recovered its original thickness upon heating. The ability to reset the height is a desirable property of the SMA spacer fabric, making it a viable option for cushioning applications and as an energy-absorbing 3D structure. SMA spacer fabrics are reusable as the samples can be reset and reused after extreme loadings. It also has enhanced performance in the hot state and absorbs more energy under significant stress than the other control samples. Also, the SMA spacer sample has a tunable performance. The stress-strain relationship and energy absorption can be tuned by controlling the temperature of the fabric. This shows

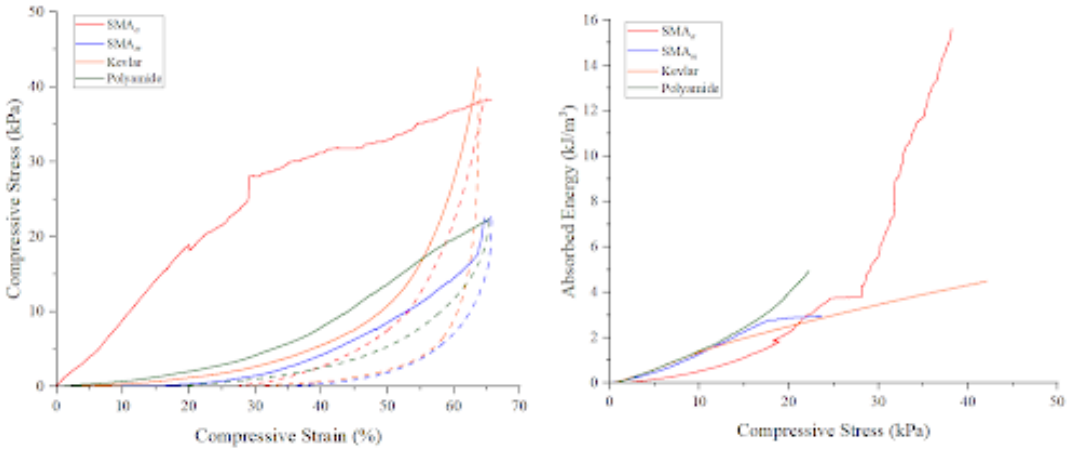

Figure 4.5: Left: Stress-strain curves for Kevlar and Polyamide control samples and SMA spacer sample, in both austenite and martensite phase. Right: Energy absorption in all the samples. SMA spacer sample in austenite has better energy absorption compared to the martensitic energy absorption

that SMA-integrated spacer fabrics have a range of applications due to their phase transitions, which we further explore through this research.

4.2 Superelastic Performance

We performed the isothermal compression test, in the hot state (120^{o}C) and cold state (20^{o}C), on all eight SMA spacer fabric samples outlined in the DOE in section 3.1.4 . Figure 4.6 shows the superelastic performance for Sample 1. Sample 1 has a fiber diameter of 0.006", tuck spacing of 0, and spacer row density of 2. When the sample is tested at 120^{o}C, in its austenite phase, the sample is stiffer than the test done at 20^{o}C, in its martensite phase. The hysteresis curve shown in red (austenite) is bigger than the hysteresis curve in blue (martensite). The sample absorbs approximately the same energy up to 30kPa. However, in the hot state, the sample can support larger stresses (up to 70kPa) and absorbs a significant amount of energy in this higher stress region. Figure 4.6 shows the energy absorption in both phases of the 3D SMA spacer fabric.

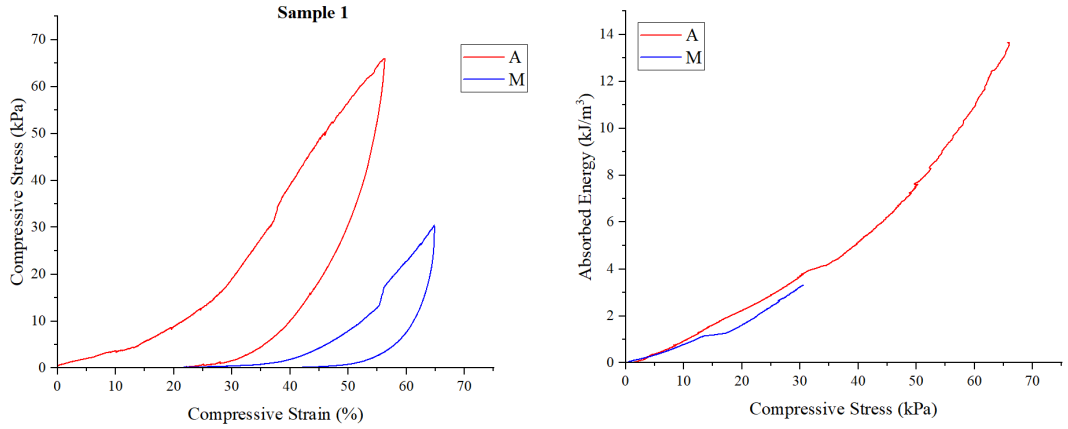

Figure 4.6: Left: Superelastic performance of Sample 1 (fiber diameter=0.006", tuck spacing =0, spacer row density=2) in austenite and martensite phases. Right: Energy absorption for Sample 1 in both the states. The sample absorbs more energy in the hot state,14kJ/m^3 compared to 3kJ/m^3 in the cold state

We saw similar trends for all the samples. Figure 4.7 shows that all the samples had a similar compression behavior. Some samples had wider hysteresis areas, showing more energy absorption than other samples. All the samples were unique, having different combinations of fiber diameter, tuck spacing and spacer row density. To analyze the effects of these individual parameters on the superelastic performance and to understand their interaction with one another, we implemented the method of averages for the DOE

analysis.

We plotted the stress-strain relationships for all the samples, comparing their superelastic performance in austenite and martensite. Figure 4.7 shows the superelastic performance for all the eight samples. We also plotted the absorbed energy vs. compressive stress for all the samples which is shown in Figure 4.8.

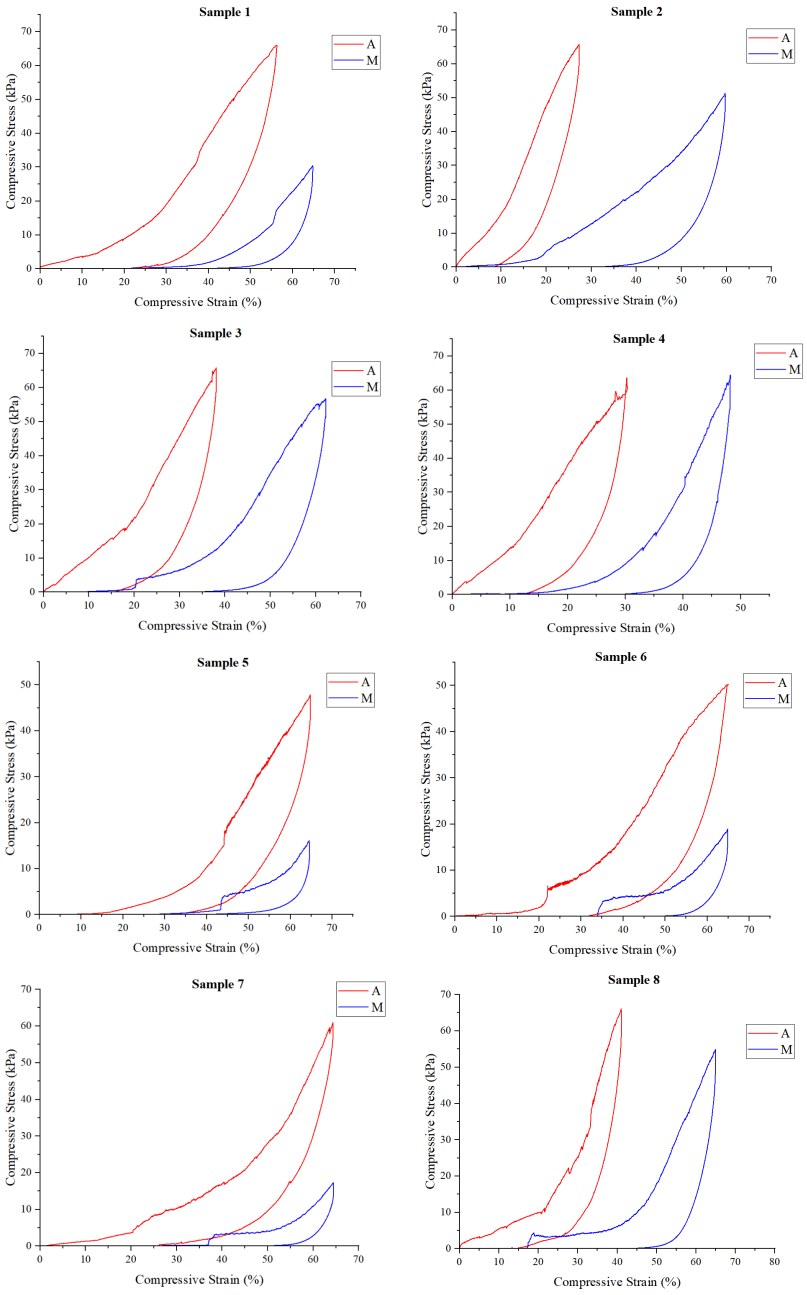

Figure 4.7: Superelastic performance for 3D SMA spacer fabric samples. The red curve shows the compression behavior in the austenite phase and the blue curve shows the compression behavior in the martensite phase.

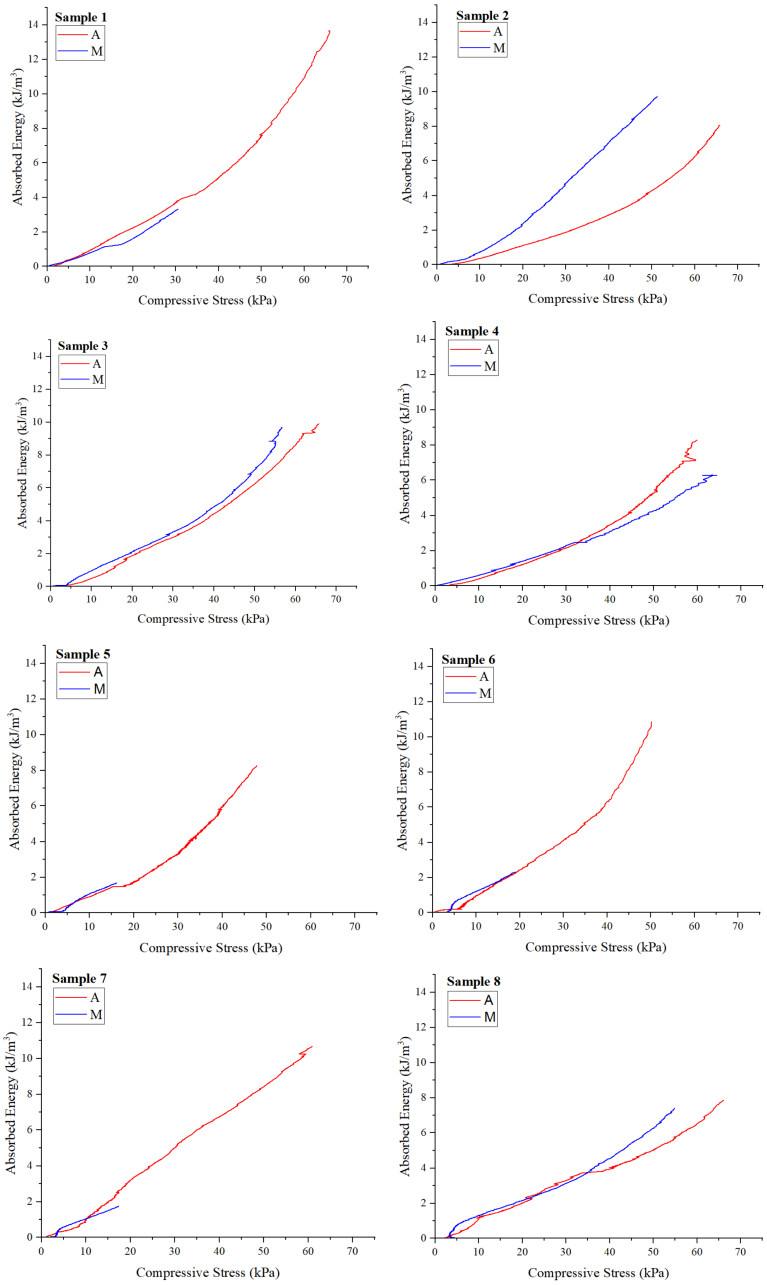

Figure 4.8: Absorbed energy vs. compressive stress for all eight samples. The red curves show the absorbed energy in austenite and the blue curve shows the absorbed energy in martensite.

4.2.1 Design of Experiments Analysis

For the DOE analysis, the method of averages was implemented. The method of averages works by averaging the data collected at the low level and subtracting it from the average of the data collected at the high level in order to calculate the effect of a factor. We identified four performance metrics, namely compressive stress, compressive strain, absorbed energy, and specific strength to evaluate the performance of these 3D SMA spacer fabrics. The calculated averages for the mentioned performance metrics are given in Table 4.1.

The compressive stress is the axial force acting on the spacer sample over the platen area. We calculate the platen area from the diameter of the platen, which was 25mm. The stress is valid only for the active region of compression, i.e. the region between the platens. The averages were calculated for the compressive stress at 20% compressive strain in austenite and the compressive stress at 40% compressive strain in martensite.

Compressive strain the change in thickness of the spacer sample during the loading and unloading cycle. It is to be noted that each sample has a different original thickness even though it has the same number of needles while knitting. The averages were calculated for the compressive strain at 30kPa compressive stress in austenite and the compressive strain at 10kPa compressive stress in martensite.

Specific strength is given by the ratio of compressive stress to the weight of the material under the platen. It is to be noted that all the samples were tested with the same 25mm platens. However, the weight of the active material (under the platen) is different for each sample due to other factors such as the fiber diameter, tuck spacing and spacer density. The averages were calculated for the specific strength for the corresponding compressive stress in austenite and the specific strength for the corresponding compressive stress in martensite.

The mechanical energy absorbed and dissipated is quantified by the area (hysteresis) between the loading and unloading curves. The absorbed energy is given by the area under the loading curve on a stress-strain curve. The averages were calculated for the absorbed energy at 30kPa compressive stress in austenite and the absorbed energy at 10kPa compressive stress in martensite.

Using the method of averages we plot the effects of individual parameters (fiber diameter, tuck spacing, spacer row density) for all the performance variables discussed above. Let us consider the energy absorption as a function of these individual parameters. Figure 4.9 shows the main effects plot for energy absorption for all the samples in the austenite and martensite phases.

From Figure 4.9, we can see that as the fiber diameter increases from 0.006" to 0.008", the energy absorption in the spacer fabric increases. Interestingly, the absorbed energy during compression increases dramatically as we increase the tuck spacing. For tuck spacing of 1, we get symmetric and equidistant "full-triangles" in the spacer architecture. For tuck spacing of 0, the spacer architecture comprises "half-triangles" that are more densely packed. From the results, we see that even with lesser material under the active region, the energy absorption becomes better. Tuck spacing 1 has a more stable geometry than tuck spacing 0. We see the same effect in the martensitic phase as well. Actually, tuck spacing is the only factor having any significant impact on the energy absorption when the sample is in the martensitic phase. However, the samples experience a decrease in energy absorption as we increase the spacer row density. This effect is prominent in the austenitic phase and is almost insignificant in the martensitic phase. In the plots, the plot line lengths demonstrate the magnitude of the impact of a particular parameter on the performance metric. The main effects for compressive stress, compressive strain and specific strength were also analyzed which are shown in Figure 4.10. Generally, as we increase the fiber diameter, the compressive stress and specific strength in the sample increase. However, we see the exact opposite trend for compressive strain. As we increase the tuck spacing from 0 to 1, the compressive stress and specific strength decrease in magnitude while the compressive strain increases. As the spacer row density increases, the compressive stress and specific strength also increase, but the compressive strain decreases.

To summarize the findings in this analysis, the tuck spacing is the main driving factor, having a significant impact on all the parameters that we studied. Hence, samples 1, 2, 3, and 4 can withstand higher forces and have higher compressive stress and specific strength than samples 5, 6, 7, and 8. This is supported by the trends we see with spacer row density and fiber diameter as well. Owing to the effect of spacer row density, samples 2 and 4 are stronger than samples 6 and 8 while samples 1 and 3 are stronger

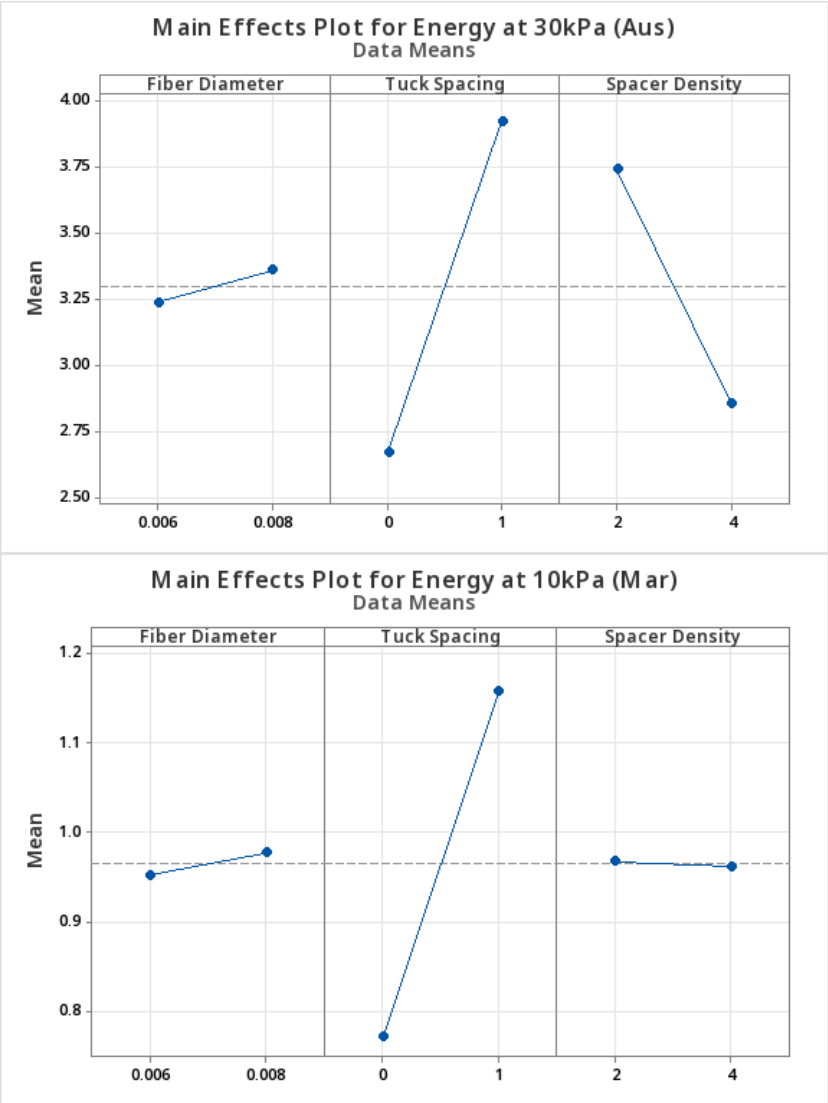

Figure 4.9: Effects of individual parameters on energy absorption

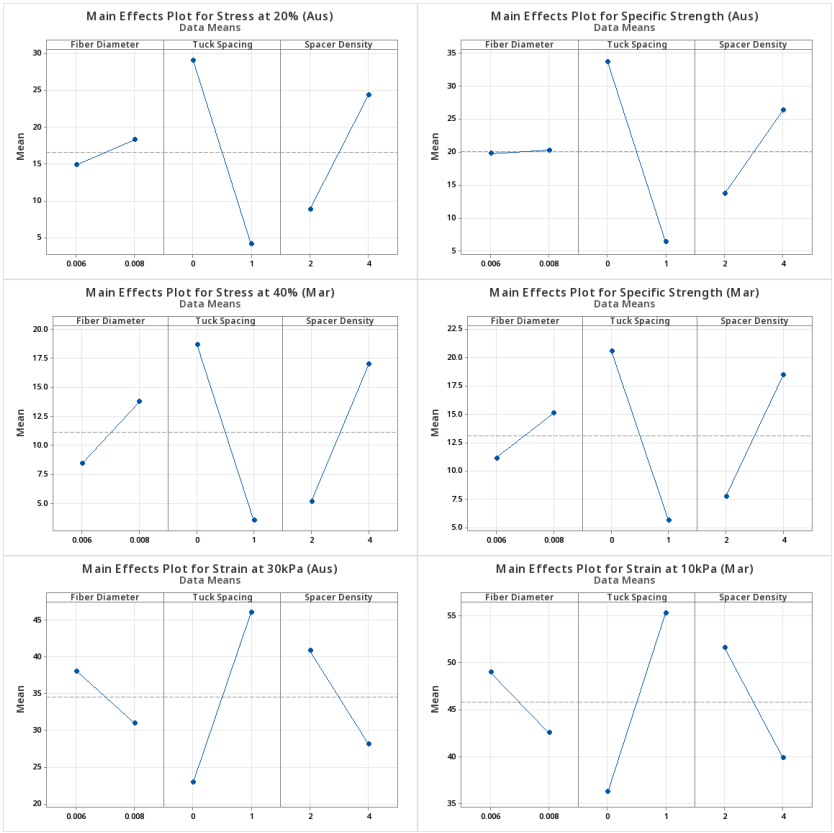

Figure 4.10: Effects of individual parameters on compressive stress, compressive strain and specific strength as performance metrics

than samples 5 and 7. Likewise, according to the effect of fiber diameter, samples 3 and 4 are stronger than samples 1 and 2 and samples 7 and 8 are stronger than samples 5 and 6. As for the deformation, tuck spacing still has the greatest impact. Samples 5, 6, 7, and 8 experience more deformation than samples 1,2,3, and 4 in both phases. The effect of fiber diameter decreases with an increase in the wire diameter. Samples 1, 2, 5 and 6 can undergo more deformation than their counterparts for both austenite and martensite phases. Similarly, samples 1,3,5, and 7, with a lower spacer row density, can withstand more deformation for a given stress value. For spacer fabrics, energy absorption is a characteristic property of their performance. We see that samples 5,6,7 and 8, with tuck spacing of 1, have better energy absorption during the compression cycle. This is the case for both austenite and martensite. Followed by the effect of tuck spacing, the spacer row density has a significant effect in austenite alone. Samples with a higher spacer row density, samples 2, 4, 6, and 8, had a decrease in energy absorption. This effect is not as pronounced in the martensite phase. With the effect of fiber diameter, we can say that samples 3, 4, 7, and 8 have slightly better energy absorption, but not as dramatic as the effect of tuck spacing.

It is important to note that we discussed how one effect alone drives the performance of the other testing parameters. This may be insufficient to draw conclusions on which factor affects the design of experiments. DOE analysis can reveal interdependencies, or interactions, between factors. With the help of interaction plots, we can analyze the competing factors for a given parameter. Each set of interactions consists of two factor pairs that are aliased by the experimental design, giving us the following interactions - fiber diameter and tuck spacing, fiber diameter and spacer row density, and tuck spacing and spacer row density.

We need to study the higher-order effects or secondary effects for all the samples and how they interact with each other. It will also allow us to identify the main driving factor in all the interdependencies. Figure 4.11 shows the interactions of the individual parameters affecting the energy absorption.

From the energy absorption interaction plots for austenite (Fig. 4.11), increasing the tuck spacing from 0 to 1 increases the energy absorption for both fiber diameters. This means that combining fiber diameter and tuck spacing can increase the energy absorption for a particular spacer fabric. We can implement these results to design 3D

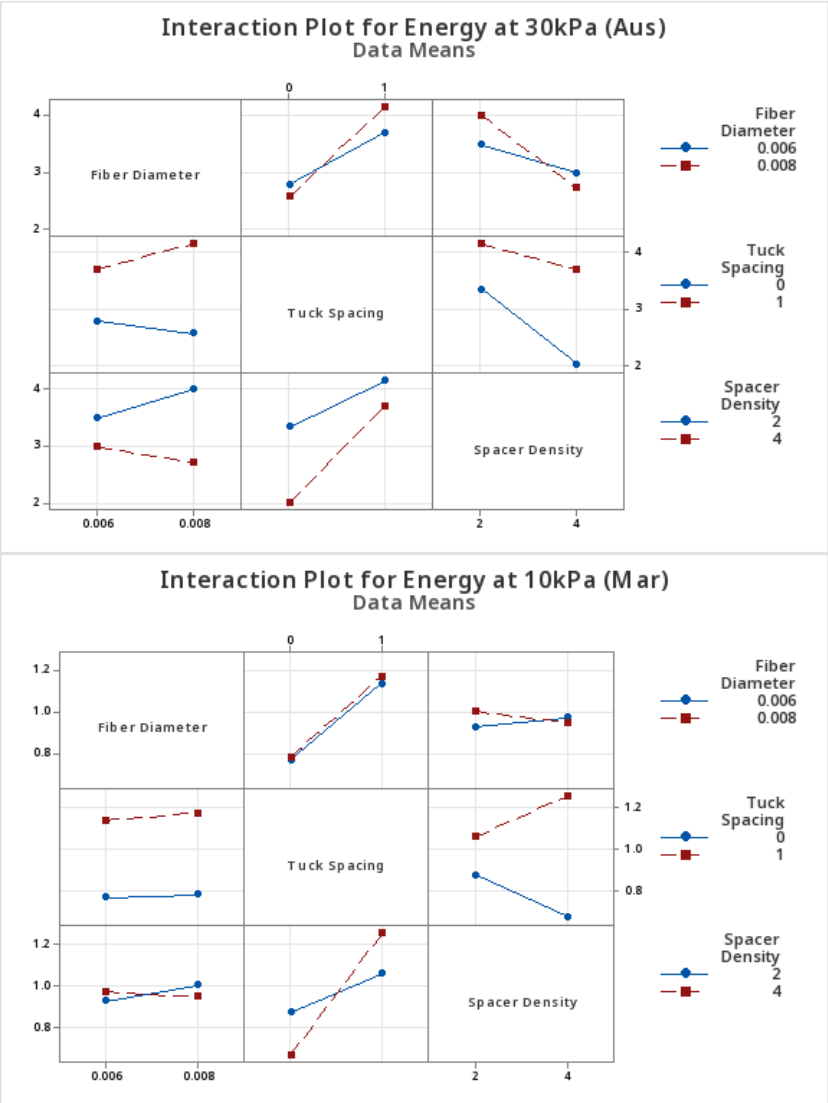

Figure 4.11: Interactions of the individual parameters affecting the energy absorption

SMA spacer fabrics with tunable energy absorption for different applications. From the same plot, we can see that combining the effect of fiber diameter and spacer row density decreases the energy absorption in the samples. Hence, spacer row density is not an appropriate tunable parameter to enhance energy absorption. For the combined effects of fiber diameter and tuck spacing and fiber diameter and spacer row density, the plot lines intersect each other. Intersecting lines tell us that these factors interact with one another, either to increase or decrease energy absorption in the samples. However, tuck spacing and spacer row density show plot lines that are almost parallel to each other. Parallel lines tell us that these two individual factors do not interact with each other. Hence, while designing energy absorbing spacer fabrics, spacer row density and tuck spacing will not contribute in enhancing the performance.

In a similar way, we studied the interaction between these individual parameters on the performance metrics of compressive stress, compressive strain and specific strength. The interaction plots for all of them are given in Figure 4.12.

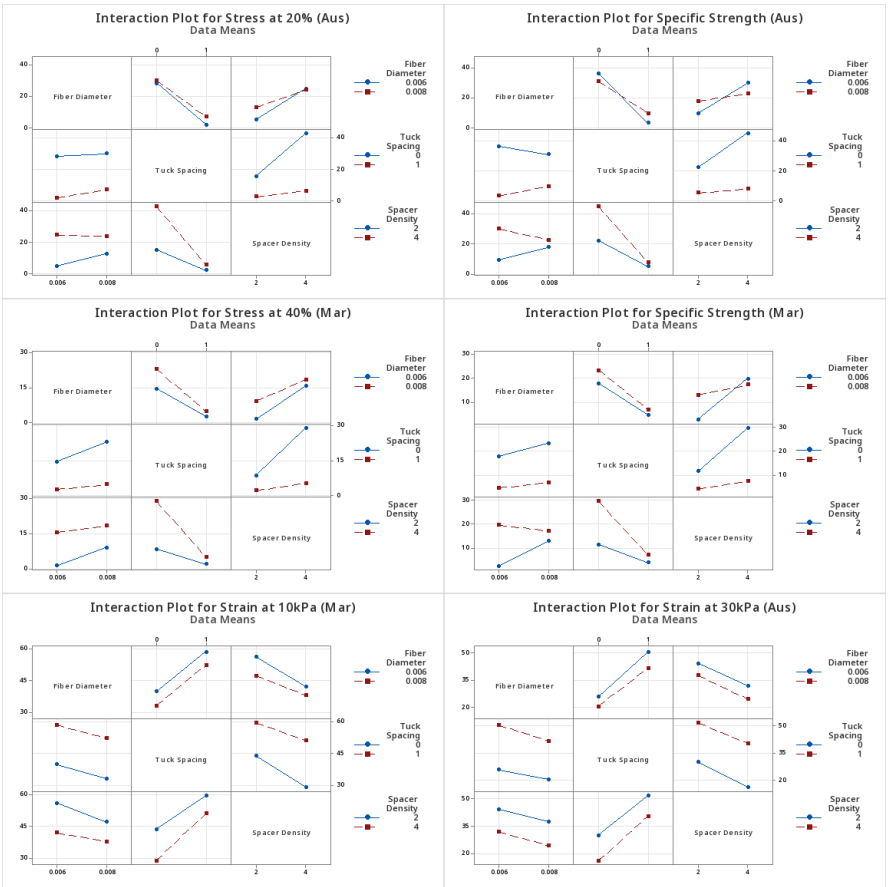

Figure 4.12: Interactions of individual parameters affecting compressive stress, compressive strain and specific strength

We evaluated all the effects and interactions of these individual parameters and isolated the impacts on the superelastic performance of 3D SMA spacer fabrics.

- From the main effects, tuck spacing is conclusively the main factor that affects the performance. Increasing the tuck spacing improves the strain and the energy absorption of the spacer fabric. On the other hand, increasing the tuck spacing decreases the stress in the samples.

- From the main effects, spacer row density also plays an important role in the performance. Increasing the spacer row density increases the stress, thus making it more stiff. This makes the samples more resistant to deformation. As the energy absorbed is dependent on the deformation in the sample, the energy absorption decreases with an increase in spacer row density.

- From the main effects, the fiber diameter has the least magnitude of impact on the performance. As expected, the stress increases with an increase in diameter and the strain decreases with an increase in diameter. As the energy absorbed is a product of stress and strain, the energy absorbed increases with an increase in spacer row density.

- From the secondary effects, fiber diameter and tuck spacing slightly increase the energy absorption when combined with each other. We don't see any significant effect in stress and strain.

- From secondary effects, fiber diameter and spacer row density together, slightly affect the strength and energy absorption of the spacer sample. The strain, however, remains unaffected.

- From secondary effects, tuck spacing and spacer row density together, improve the stress and energy absorption. Again, strain does not get impacted by this combination

4.2.2 Effects of Different Strain Rates on Energy Absorption

In the previous section, we investigated the effects of fiber diameter, tuck spacing, and spacer row density on the superelastic performance of SMA spacer samples. It would be interesting to see if the spacer fabrics showed different superelastic behavior depending on the testing protocol. For the isothermal compression test, we kept the strain rate constant for all the samples. To study the effect of different strain rates, we chose sample 5 from the DOE. We created four additional samples, which gave us five samples in total. They were called 5.1, 5.2, 5.3, 5.4 and 5.5. Here, sample 5.1 is the same sample used in the DOE in section 4.2.1. For the test run, the isothermal compression test was conducted at 120^oC, only for the austenite phase. We have Figure 4.13 with samples 5.3, 5.4, and 5.5. In this comparison, for a given rate of compression, the samples have a similar stress-strain behavior. We can see that the hysteresis curve for the fast rate ($4x10^-2s^-1$) is wider, and more open compared to the curves for the slow ($4 \text{ x } 10^-4s^-1$) and medium ($5.5x10^-3s^-1$) rates. Hence, the samples tested at a faster rate were stiffer. From the energy absorption plots in Figure 4.13, we can see that the absorbed energy increases with increased strain rates. The energy absorbed during the fast rate of compression is 6.86 kJ/m^3 for Sample 5.5, whereas it is 4.1 kJ/m^3 for the slow rate of compression.

From these results, we can conclude that increasing the compression rate while testing, increases the stiffness in the spacer fabric. Hence, the energy absorption also increases with the increase in the rate of compression for a given spacer fabric.

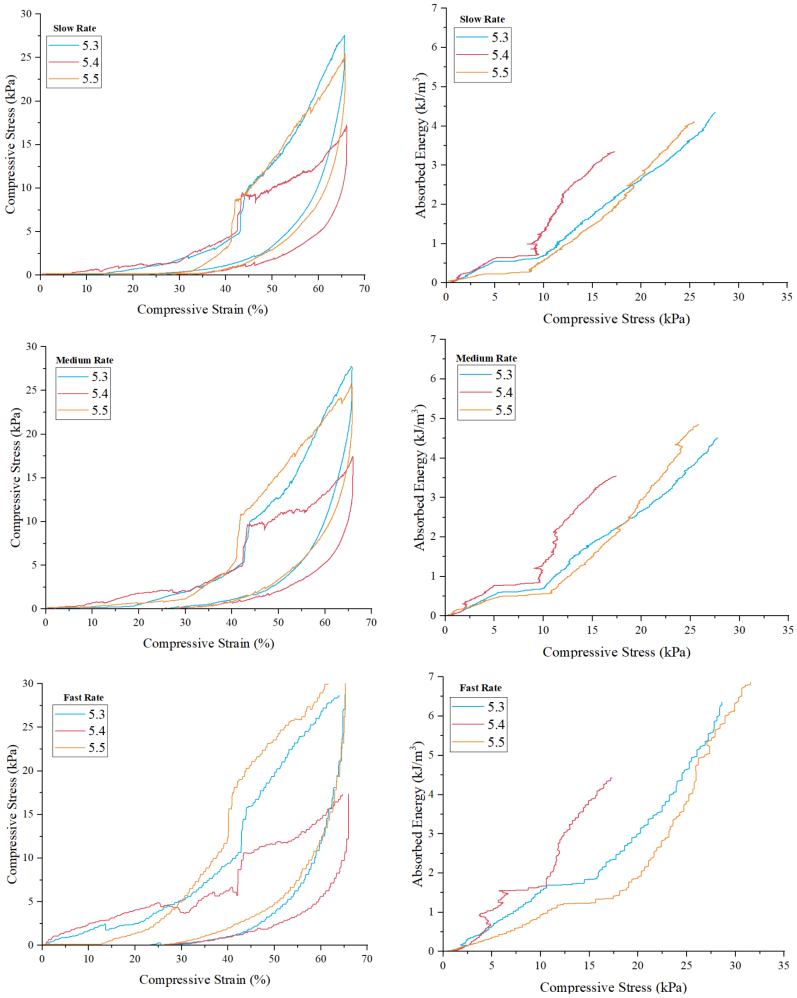

Figure 4.13: Stress-strain relationships and energy absorption for Samples 5.3, 5.4 and 5.5 tested at three different rates of compression.

Sample	Fiber Diameter	Tuck Spacing	Spacer Row Density	Stress at 20% (A)	Stress at 40% (M)	Specific Strength (A)	Specific Strength (M)	Strain at 30kPa (A)	Strain at 10kPa (M)	Absorbed Energy at 30kPa (A)	Absorbed Energy at 10kPa (M)
1	-	-	-	8.86	1.15	16.24	3.39	36.40	52.37	3.68	0.79
2	-	-	+	47.57	27.05	56.63	32.20	14.92	26.84	1.87	0.74
3	+	-	-	21.76	15.03	28.37	19.60	23.62	35.16	2.99	0.96
4	+	-	+	37.97	30.88	33.41	27.17	17.08	30.74	2.15	0.60
5	-	+	-	1.22	0.70	2.96	1.70	52.10	59.77	3.29	1.07
6	-	+	+	1.94	4.20	3.35	7.25	48.87	57.12	4.11	1.21
7	+	-	-	3.68	3.22	7.23	6.33	51.47	59.25	5.01	1.05
8	+	+	+	9.93	6.03	12.14	7.37	31.82	45.08	3.29	1.30

Table 4.1: Performance metrics for the DOE analysis

4.3 Shape Memory Effect

We performed the constant force temperature ramp test on all the eight samples to study the shape memory effect of 3D SMA spacer fabrics. Let's consider Sample 1 (fiber diameter = 0.006", tuck spacing = 0, spacer row density = 2) shown in Figure 4.14 for the shape memory effect discussion.

The plot shows six different constant force values (0.5N, 1N, 2N, 3N, 4N and 5N) with the solid red triangle as the initial hot state (at 120^oC, A1), blue solid square as the cold state (at 20^oC, M) and then the red solid circle as the last hot state (at 120^oC, A2). For a given force value, the sample goes from A1 temperature to M temperature, undergoing change in gap height (strain). At the same force, the sample recovers the change in height when the temperature increases from M to A2. We can see that the spacer fabric does mechanical work with the temperature fluctuation, hence showing actuation in the sample. We calculated the actuation displacement for Sample 1, shown in figure 4.15. The plot shows an "actual" displacement curve that was derived from the actual testing data discussed in fig. 4.15. The plot also shows a "theoretical" displacement curve derived from discretizing the forces in the austenite and martensite loading curves from the isothermal compression test. The theoretical displacement curve is only used to depict the "ideal" shape memory effect of the spacer fabric.

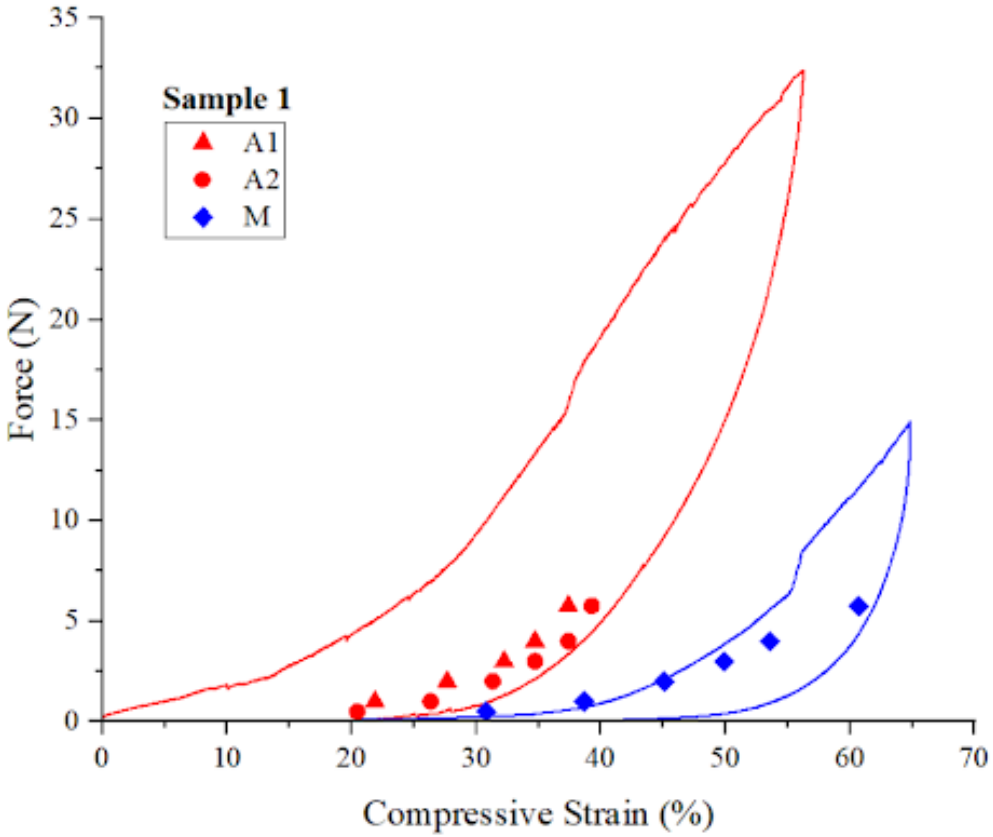

Figure 4.14: Shape memory effect seen in sample 1

From fig. 4.15, we can see the maximum actual displacement in sample 1 is about 2 mm at 5N. We can say that this spacer fabric can actuate up to 2 mm while doing mechanical work against a constant 5N force.

In this manner, we can evaluate the shape memory effect of all the spacer fabric samples. Figure 4.16 shows the constant force temperature ramp test plotted on the isothermal compression plots and figure 4.17 shows the actuator curves for all the samples.

To understand the effects of fiber diameter, tuck spacing and spacer row density on the actuation displacement, we need to conduct a DOE analysis.

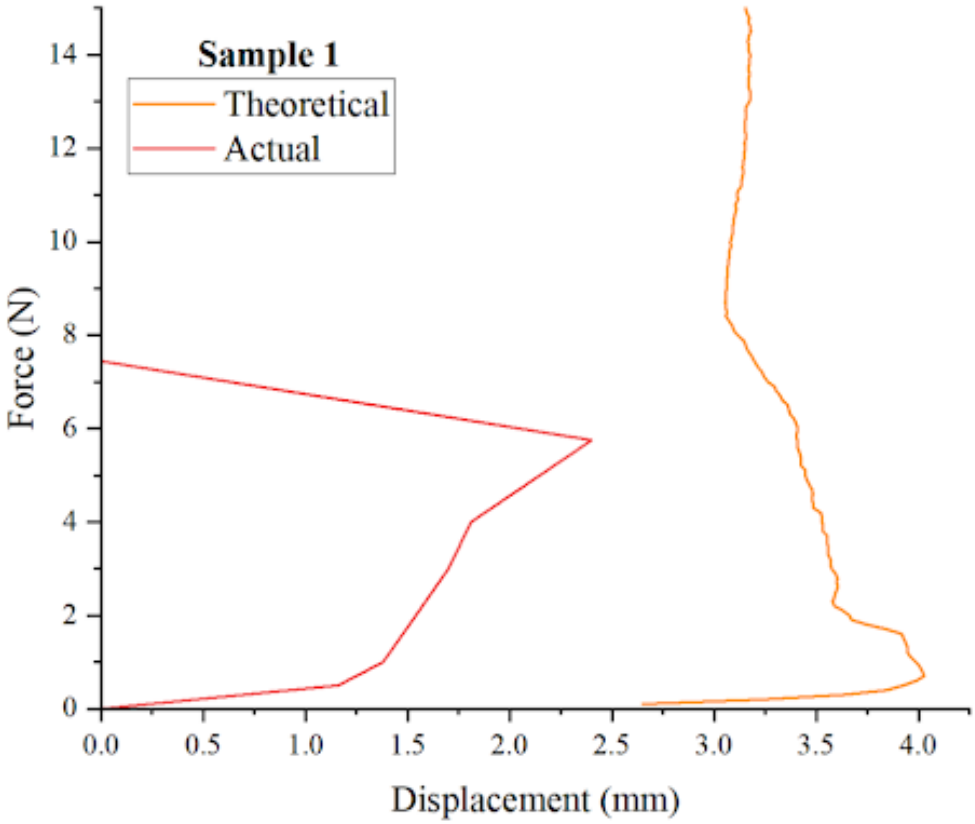

Figure 4.15: Actuator curves for Sample 1

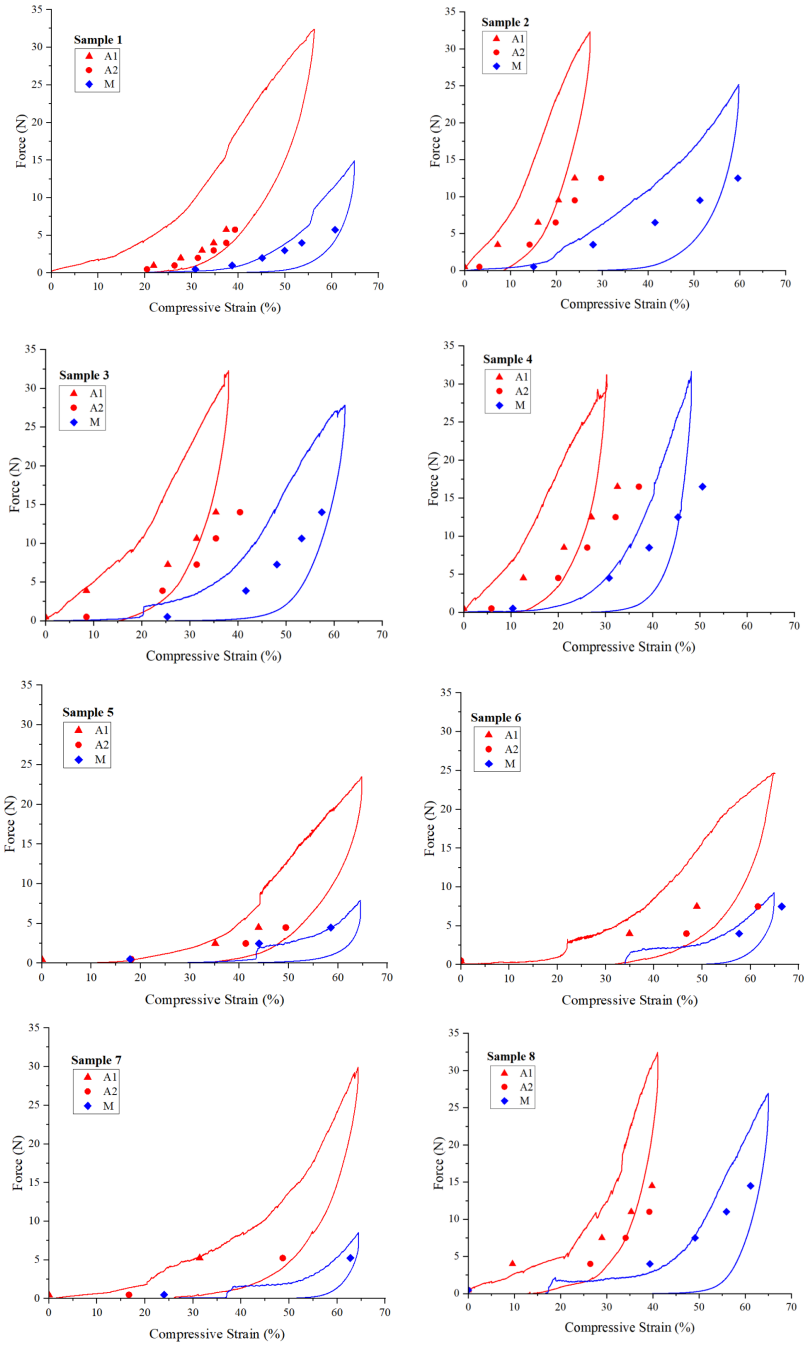

Figure 4.16: Constant force temperature ramp test plotted on the isothermal compression plots

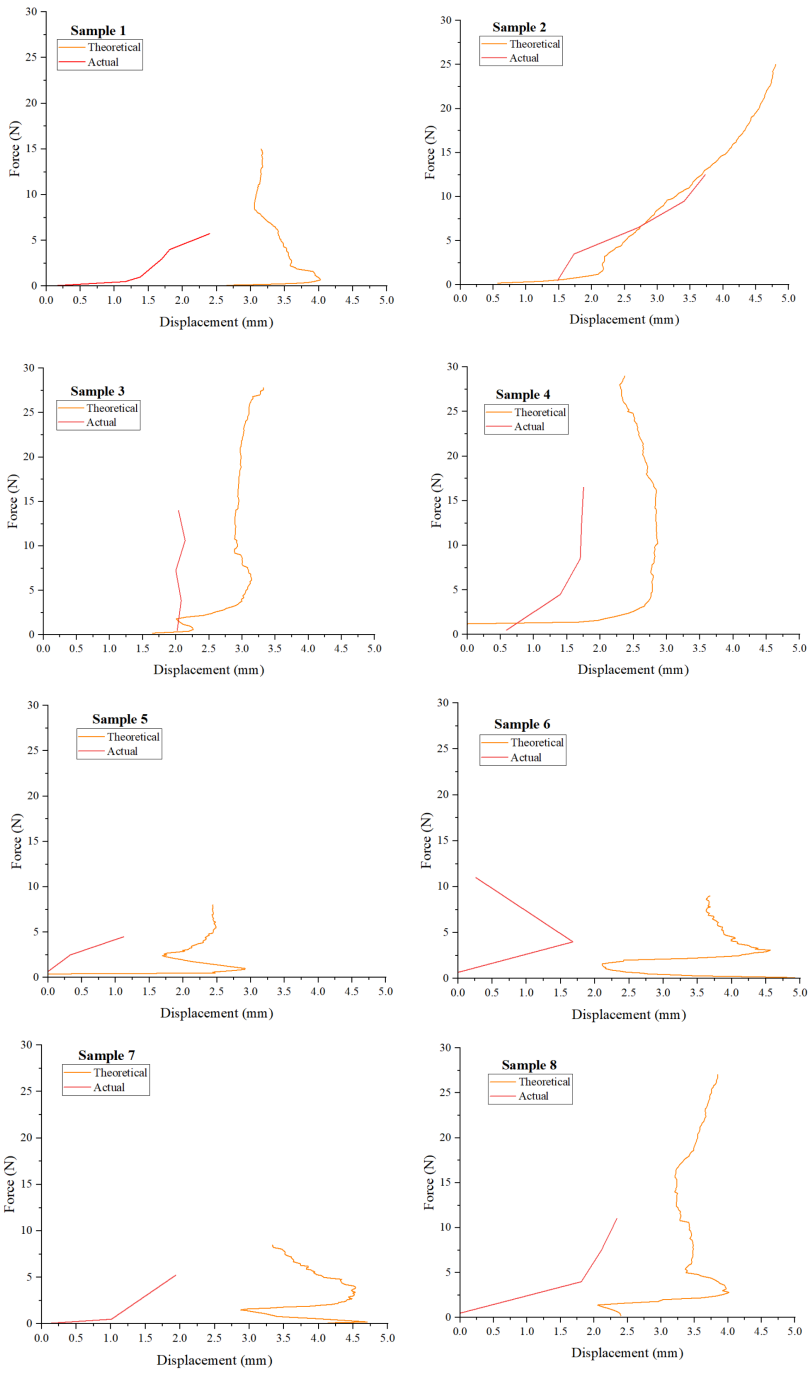

Figure 4.17: Actuator curves showing “actual” and “theoretical” displacement

4.3.1 Design of Experiments Analysis

Now that we got the actuator curves for all the samples, to evaluate the shape memory effect for these spacer fabrics, we needed to run a full factorial DOE. For the DOE run, the actual experimental data alone was used. Similar to the isothermal DOE run, we studied the main effects of the three main factors, the fiber diameter, tuck spacing and spacer row density.

For the individual parameters, the actual displacement at 5N force was used for the evaluation of the effects. Again, the method of averages was used to plot the main effects and their interactions. Figure 4.18 shows the effects of individual parameters on actuator displacement.

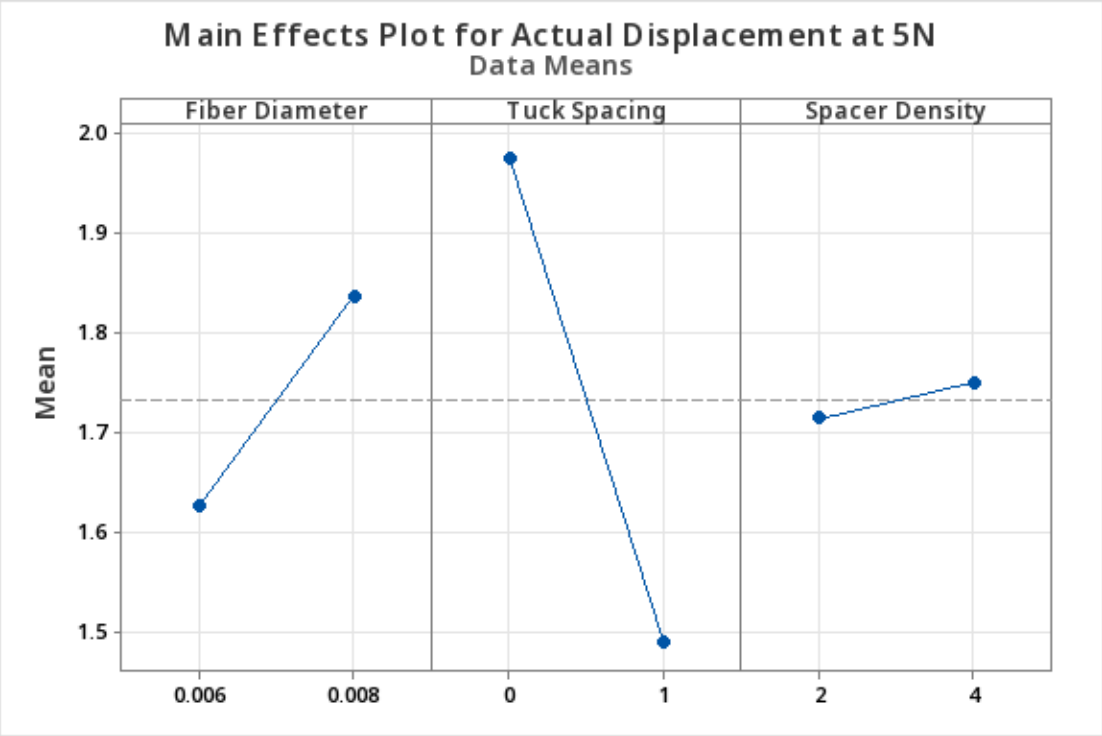

Figure 4.18: Effects of individual parameters on actuator displacement

We can see that, as we increase the fiber diameter the actuation in the fabric increases. However, as we increase the tuck spacing from 0 to 1, the ability of the samples to actuate or recover their thickness decreases. Increasing the spacer row density increases the actuation, but is not as dramatic. From the main effects plots, we can say that the most impact on the actuation potential is tied to the tuck spacing of the fabrics. From these observations, we can conclude that a sample with a higher fiber diameter and a lower tuck spacing has better actuation potential than other samples. Samples 3 and 4, figuratively, should have better actuation over the other samples. If we consider the effect of spacer row density as well, sample 4 is superior to sample 3.

In order to draw solid conclusions, we need to study the secondary effects for these parameters. In figure 4.19, we can see the interdependencies of these individual factors and their interactions will help us better understand the shape memory effect in our design.

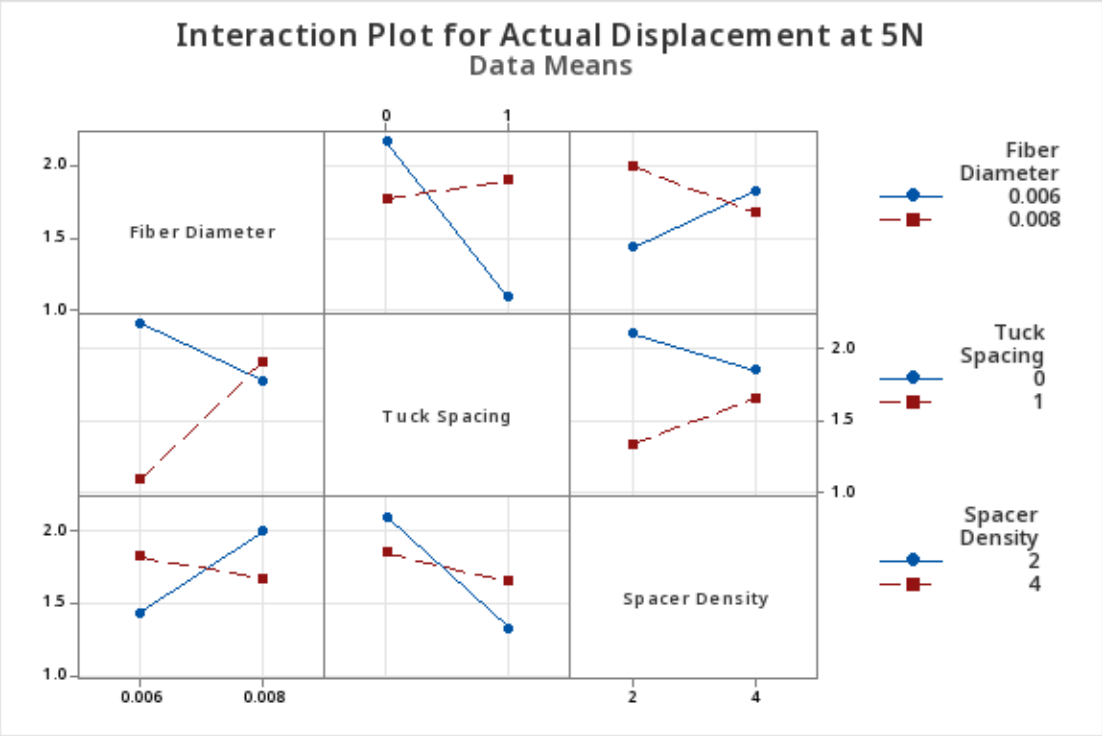

Figure 4.19: Secondary interactions of individual parameters for the actuator displacement of the spacer fabric samples

As seen in the interaction plot for actual displacement at 5N, fiber diameter / tuck spacing interact with each other, showing a combined effect on the actuation in the fabric. However, as we increase the tuck spacing, the actuation decreases in samples having the lower fiber diameter (0.006"). Samples made from the 0.008" wire do not see a stark increase in actuator displacement by combining fiber diameter / tuck spacing. We can also see a strong interaction between fiber diameter / spacer row density, where lower diameter samples show better actuation by increasing the row density. We don't see a combined effect of tuck spacing / spacer row density on the actuator displacement in the samples.

We evaluated the effect of individual parameters and their interaction with one another and we can conclude the following:

- Increasing the fiber diameter increases the actuation displacement in the 3D SMA spacer fabrics.

- Increasing the tuck spacing decreases the actuation displacement in the 3D SMA spacer fabrics.
- Increasing the spacer row density slightly increases the actuation displacement in the spacer fabric.

Chapter 5

Conclusion

This chapter summarizes the contributions of this research on 3D SMA spacer fabrics. This section outlines the accomplishment of the research objectives defined in Section 1.4. The goal of this research was to investigate the impact of textile design (material, geometry, manufacturing) and SMA behaviors (superelasticity and shape memory effect) on the mechanical performance of 3D SMA spacer fabrics.

With this research, we were able to successfully fabricate a 3D SMA spacer fabric. The manufacture was done manually on a flat-bed weft knitting machine in the Design of Active Materials and Structures Laboratory. The fabrication of these 3D SMA spacer fabrics was especially challenging as it is not very common to manufacture spacer fabrics on a weft knitting machine. The process combining circular knitting along with the tuck operation was authentically developed by me, which I have documented in this research.

With this research, we established testing protocols to investigate energy absorption and actuation in 3D SMA spacer fabrics. As per my literature review, standards for testing 3D SMA spacer fabrics are not available. There exist different testing protocols and ASME standards to test 3D spacer fabrics. Integration of SMA in 3D spacer fabrics is a novel research approach and it is still in its nascent stage. There is immense potential in this design space and over time, there will be standard tests to evaluate the compression behavior of 3D SMA spacer fabrics.

With this research, we were able to show actuation in 3D SMA spacer fabrics. I think this was a main contribution from this research. Using 3D SMA spacer fabrics as actuators adds another dimension of functionality to conventional SMA actuators.

These spacer fabrics show a unique duality due to SMA, where superelasticity makes them good energy absorbing materials and shape memory effect opens a new avenue for 3D SMA actuator fabrics.

Lastly, we showed the impacts of different geometric parameters on superelasticity and shape memory effect in 3D SMA spacer fabrics. We were able to identify tunable material, geometric and manufacturing parameters and explore the new design space for 3D SMA spacer fabrics. We were successfully able to isolate the individual impacts of design parameters (fiber diameter, tuck spacing and spacer row density) and evaluate their interdependence on each other.

This research paves way in the foundational understanding of 3D shape memory alloy spacer fabrics. Owing to the SMA behaviors of superelasticity and shape memory effect, this research deems 3D SMA spacer fabrics as good energy absorbing structures to enhance human health and wellbeing.

Chapter 6

Future Work

This research provides fundamental information for the design, fabrication and analysis of 3D SMA spacer fabrics. The scope of this research was limited to master's level thesis and it has a lot of potential for future research.

Firstly, there are better and more accurate methods for fabrication of spacer fabrics. Warp knitting is the industry standard for making spacer fabrics and it will definitely be a more suitable option for making SMA-based spacer fabrics. It will ensure precision and programmability allowing the incorporation of more design parameters into the spacer architecture with a higher throughput. With that being said, the flat-bed weft knitting machine used had fixed constraints such as the needle spacing, needle alignment and the distance between the beds. It was also not possible to make spacer fabrics with greater values of tuck spacing due to some physical constraints on the machine.

Integration of different SMA yarns and fibers in the spacer fabric architecture can enhance their performance. It would be worthwhile to explore SMA wire inlays to improve the cushioning behavior of 3D SMA spacer fabrics. Using SMA wires with different transition temperatures can make more functional 3D spacer fabrics that can be used in specific applications. SMA yarns in the spacer architecture can make them easy to manufacture and can be used as wearables.

As per the manufacturing method used, such 3D textiles can have added functionality by identifying different design variables. We can alter the thickness of these fabrics by changing the machine parameters. We can explore a new array of geometric variations in the spacer architecture that would enable us to make advanced energy absorbing

spacer fabrics.

References

[1] Nathan Brown, Meredith K Owen, Anthony Garland, John D DesJardins, and Georges M Fadel. Design of a single layer metamaterial for pressure offloading of transtibial amputees. *Journal of Biomechanical Engineering*, 143(5):051001, 2021.

[2] Vimal Dhokia, James Bilzon, Elena Seminati, David Canepa Talamas, Matthew Young, and William Mitchell. The design and manufacture of a prototype personalized liner for lower limb amputees. *Procedia CIRP*, 60:476–481, 2017.

[3] Brian J Hafner, John C Cagle, Katheryn J Allyn, and Joan E Sanders. Elastomeric liners for people with transtibial amputation: Survey of prosthetists' clinical practices. *Prosthetics and orthotics international*, 41(2):149–156, 2017.

[4] Thomas Michael Seigler. *A comparative analysis of air-inflated and foam seat cushions for truck seats*. PhD thesis, Virginia Tech, 2002.

[5] Yan Guo, Lin Chen, Sheng Qiang, Xian Qian, Tao Xue, and Fang He. Comparing properties of the warp-knitted spacer fabric instead of sponge for automobile seat fabric. In *Journal of Physics: Conference Series*, volume 1948, page 012196. IOP Publishing, 2021.

[6] Gregory S Walsh and Daniel C Low. Military load carriage effects on the gait of military personnel: A systematic review. *Applied ergonomics*, 93:103376, 2021.

[7] Joseph J Knapik, Katy L Reynolds, and Everett Harman. Soldier load carriage: historical, physiological, biomechanical, and medical aspects. *Military medicine*, 169(1):45–56, 2004.

[8] Kimberley A Andersen, Paul N Grimshaw, Richard M Kelso, and David J Bentley. Musculoskeletal lower limb injury risk in army populations. *Sports medicine-open*, 2:1–9, 2016.

[9] Robin Marc Orr, Rodney Pope, Julia Coyle, and Venerina Johnston. Occupational loads carried by australian soldiers on military operations. *J Health Saf Environ*, 31(1):451–67, 2015.

[10] David Boffey, Idan Harat, Yftach Gepner, Cheyanne L Frosti, Shany Funk, and Jay R Hoffman. The physiology and biomechanics of load carriage performance. *Military medicine*, 184(1-2):e83–e90, 2019.

[11] Bernard Liew, Susan Morris, and Kevin Netto. The effect of backpack carriage on the biomechanics of walking: A systematic review and preliminary meta-analysis. *Journal of applied biomechanics*, 32(6):614–629, 2016.

[12] Robin Marc Orr, Rodney Pope, Venerina Johnston, and Julia Coyle. Soldier occupational load carriage: a narrative review of associated injuries. *International journal of injury control and safety promotion*, 21(4):388–396, 2014.

[13] Georgia Melia, Petros Siegkas, Jodie Levick, and Charlotte Apps. Insoles of uniform softer material reduced plantar pressure compared to dual-material insoles during regular and loaded gait. *Applied Ergonomics*, 91:103298, 2021.

[14] Tong Li and Qingguo Li. A systematic review on load carriage assistive devices: Mechanism design and performance evaluation. *Mechanism and Machine Theory*, 180:105142, 2023.

[15] Ming Hao, Jiwen Zhang, Ken Chen, Harry Asada, and Chenglong Fu. Supernumerary robotic limbs to assist human walking with load carriage. *Journal of Mechanisms and Robotics*, 12(6):061014, 2020.

[16] Guldemet Basal and Sevcan Ilgaz. A functional fabric for pressure ulcer prevention. *Textile Research Journal*, 79(16):1415–1426, 2009.

[17] R Roaf. The causation and prevention of bed sores. In *Bed sore biomechanics*, pages 5–9. Springer, 1976.

[18] Xiaohua Ye, Hong Hu, and Xunwei Feng. Development of the warp knitted spacer fabrics for cushion applications. *Journal of industrial textiles*, 37(3):213–223, 2008.

[19] Yanping Liu and Hong Hu. Compression property and air permeability of weft-knitted spacer fabrics. *The Journal of the Textile Institute*, 102(4):366–372, 2011.

[20] Shuang Yu, Mancheng Dong, Gaoming Jiang, and Pibo Ma. Compressive characteristics of warp-knitted spacer fabrics with multi-layers. *Composite Structures*, 256:113016, 2021.

[21] Nga-wun Li, Kit-lun Yick, and Annie Yu. Novel weft-knitted spacer structure with silicone tube and foam inlays for cushioning insoles. *Journal of Industrial Textiles*, 51(4_suppl):6463S–6483S, 2022.

[22] Qianwen Wang, Xiao Peng, Yan Zu, Lili Jiang, and Kai Dong. Scalable and washable 3d warp-knitted spacer power fabrics for energy harvesting and pressure sensing. *Journal of Physics D: Applied Physics*, 54(42):424006, 2021.

[23] Mohsen Hamedi, Parisa Salimi, and Nima Jamshidi. Improving cushioning properties of a 3d weft knitted spacer fabric in a novel design with niti monofilaments. *Journal of industrial textiles*, 49(10):1389–1410, 2020.

[24] John A Shaw et al. Tips and tricks for characterizing shape memory alloy wire: part 1—differential scanning calorimetry and basic phenomena. 2008.

[25] Ashwin Rao, Arun R Srinivasa, and Junuthula Narasimha Reddy. *Design of shape memory alloy (SMA) actuators*, volume 3. Springer, 2015.

[26] KH Eckelmeyer. Effect of alloying on the shape memory phenomenon in nitinol. *Scr. Metall.;(United States)*, 10(8), 1976.

[27] Charles Aaron Weinberg. *Functionalized Shape Memory Alloy Microfilament Twisted Yarn Structures*. PhD thesis, University of Minnesota, 2021.

[28] Joanne Yip and Sun-Pui Ng. Study of three-dimensional spacer fabrics:: Physical and mechanical properties. *Journal of materials processing technology*, 206(1-3):359–364, 2008.

[29] Lea Albaugh, James McCann, Scott E Hudson, and Lining Yao. Engineering multifunctional spacer fabrics through machine knitting. In *Proceedings of the 2021 CHI Conference on Human Factors in Computing Systems*, pages 1–12, 2021.

[30] MIAO Xu-hong and Ge Ming-Qiao. The compression behaviour of warp knitted spacer fabric. *Fibres Text East Eur*, 16(1):90–92, 2008.

[31] Kevin Paul Eschen. *Multiscale Mechanics of Shape Memory Alloy Knitted Architectures*. PhD thesis, University of Minnesota, 2020.